

The singularity index for soil geochemical variables, and a mixture model for its interpretation

R.M. Lark^{1*}, M. Patton², E.L. Ander¹, D.M. Reay²

¹*British Geological Survey, Keyworth, Nottinghamshire NG12 5GG, U.K.* ²*Geological Survey of Northern Ireland, Dundonald House, Upper Newtownards Road, Ballymiscaw, Belfast BT4 3SB, U.K.*

1

2 Abstract

3 A geochemical anomaly is a concentration of an element or other constituent in a
4 medium (soil, sediment or surface water) which is unusual in its local setting. Geochemi-
5 cal anomalies may be interesting as indicators of processes such as point contamination or
6 mineralizations. They may therefore be practically useful, indicating sources of pollution
7 or mineral deposits which may be of economic value. As defined, a geochemical anomaly
8 is not merely a large (or small) concentration of a constituent as compared to the marginal
9 distribution. To detect anomalies we must therefore do more than simply map the spatial
10 distribution of the constituent. One proposed approach makes use of a singularity index
11 based on fractal representation of spatial variation. The singularity index can be com-
12 puted from local concentration measures in nested windows. In this paper we propose an
13 approach to compute threshold values for the index to identify enrichment and depletion
14 anomalies, separate from background information. The approach is based on a mixture
15 model for the singularity index, and it can be supported by computing a distribution for
16 background values of the index by parametric bootstrapping from a robustly-estimated
17 variogram model for the target constituent. This approach is illustrated here using data
18 on elements in the soil in four settings in Great Britain and Ireland.

19 Keywords. Geochemistry; Anomalies; Singularity; Fractal; Mixture model

20

*Now at University of Nottingham, Sutton Bonington Campus, Sutton Bonington, LE12 5RD, U.K.
E-mail address: murray.lark@nottingham.ac.uk (R.M. Lark).

21 **1. Introduction**

22 *1.1 The problem*

23 Soil geochemical data comprises information on the concentration of elements in soil
24 (e.g. heavy metals, micronutrients such as selenium and potentially harmful elements such
25 as As), compounds (e.g. specific organic pollutants, ions such as nitrate or phosphate)
26 and other constituents such as organic carbon. The soil may be a convenient medium for
27 geochemical survey (e.g. Breward, 2007) focussed on mineral exploration or to support ge-
28 ological mapping. Soil geochemical data may also support the management of agricultural
29 soils (e.g. Lark et al., 2014) or the assessment of particular threats to soil quality (e.g.
30 Rawlins et al., 2006). In all cases a common objective in the analysis of soil geochemical
31 data (as with data in other media such as stream sediments), is the identification of anoma-
32 lies. A geochemical anomaly is a measurement, or local cluster of measurements, which
33 have markedly large or small concentrations in local context. Anomalies may be impor-
34 tant as indicators of mineralizations which could be economically important, or they may
35 reflect point pollution processes which must be understood for environmental protection.

36 The detection of anomalies requires more than the mapping of large or small con-
37 centrations. Rather it is the identification of local accumulation or depletion which is
38 anomalous in context. One method that has been used to tackle this problem invokes
39 a multifractal model of spatial variation under which variation may include local singu-
40 larities (e.g. Chen et al., 2007). This paper proposes an approach to the detection of
41 anomalies in data on soil which is based on this method. The next section outlines the
42 approach based on singularities in more detail. The methods used in this paper are then
43 described (section 2.1) and then applied in four case studies on concentrations of elements
44 in four contrasting settings in the United Kingdom and Ireland.

45 *1.2 Anomalies and singularities*

46 In the approach to anomaly detection based on a multifractal model the local
47 anomalous accumulation of material (or equivalently, depletion), arising from local het-

48 erogeneities or cascade processes is treated as a *singularity* characterized by the local
 49 singularity index. A fuller account of the underlying theory is given by Cheng (2007;
 50 2012) and Agterberg (2012), but we summarize here.

51 We denote a local support in d dimensions (e.g. a square or circle when $d = 2$)
 52 centred at location \mathbf{x} and of (linear) size ε by $\mathcal{B}_{\mathbf{x}}(\varepsilon)$. The amount of some material
 53 within the support, $\mu(\mathcal{B}_{\mathbf{x}}(\varepsilon))$ depends on the local background concentration $c(\mathbf{x})$ scaled
 54 according to a local singularity index, $\alpha(\mathbf{x})$:

$$\mu(\mathcal{B}_{\mathbf{x}}(\varepsilon)) = c(\mathbf{x})\varepsilon^{\alpha(\mathbf{x})}. \quad (1)$$

55 The equivalent expression for the mean concentration over the support is

$$\rho(\mathcal{B}_{\mathbf{x}}(\varepsilon)) = c(\mathbf{x})\varepsilon^{\alpha(\mathbf{x})-d}. \quad (2)$$

56 Allégre and Lewin (1995) reviewed the range of processes which give rise to observed
 57 distributions of geochemical variables. In many cases a normal or log-normal distribution
 58 may be expected under which the expected value of $\alpha(\mathbf{x})$ over a domain of interest is equal
 59 to d . In the presence of local anomalies, however, the variation is multifractal with local
 60 values of $\alpha(\mathbf{x}) < d$ where there is local enrichment of the material of interest and $\alpha(\mathbf{x}) > d$
 61 where there is depletion.

62 For a multifractal process the set of points with a particular singularity index value
 63 itself constitutes a fractal set. This provides the basis for the practical approach taken to
 64 the identification of anomalies from the singularity index by the concentration-area model
 65 (Cheng, 2012). Under this model the area over which the singularity index is larger than
 66 some value, α , $A[> \alpha]$, the survival function of α , follows a power-law,

$$A[> \alpha] \propto \alpha^{-\beta}, \quad (3)$$

67 although there may be several values of β over distinct sub-ranges of the value of α . When
 68 the survival function is plotted on double-log axes these ranges should be revealed as linear
 69 segments of the plot. Liu et al. (2014) fit such linear segments and, from the break-points

70 between them, identify a range of values of α which correspond to the background process
71 and limits which define the range for enrichment and depletion anomalies respectively.

72 In this paper we consider case studies in which the singularity index was computed
73 for the concentration of different elements in the topsoil across four different areas. In no
74 case did the double-log plot of the empirical survival function of α clearly resemble a limited
75 number of linear segments, rather, like any non-linear plot, it could be approximated to
76 some arbitrary degree of accuracy by increasing numbers of such segments (see Figure
77 26) which makes the outcome for the range of values of the index assumed to correspond
78 predominantly to background normal or log-normal variation essentially arbitrary. This
79 is unsatisfactory. For this reason we propose an alternative approach. The singularity
80 index under the normal or log-normal monofractal background model is assumed to have
81 a distribution conditional on the spatial correlation of the variable, the distribution of
82 the sample points and the scales examined. It is assumed that the distribution of the
83 index for the whole field can be represented as a mixture of normal distributions, of
84 which the dominant component represents the background. The mixture also includes
85 one or more additional components which introduce mass into one or both tails of the
86 overall distribution, representing anomalies. Note that previous workers have used mixture
87 models for the concentrations of elements in soil to represent background and anomalous
88 concentrations (e.g. Liu et al., 2010). It is important to remember that, in this paper,
89 we model the singularity index rather than the concentrations themselves as a mixture of
90 components.

91 In the remainder of the paper we describe the methods used and outline the results
92 for the case studies.

93 **2. Materials and Methods**

94 *2.1 Computation*

95 The data used in this paper are described in detail in sections 2.2–2.5. In all cases

96 the data were total concentrations of an element in the topsoil (soil to a depth of 15 cm
97 from the surface). As described for each section, summary statistics and histograms of the
98 data were obtained, and a decision was made as to whether a transformation was required
99 prior to geostatistical analysis to ensure the plausibility of an assumption of normality
100 (although the computation of the singularity index was done on the data on their original
101 units of measurements, mg kg^{-1}).

102 *2.1.1 The singularity index.* In all case studies the singularity index was computed on
103 the nodes of a 100-m square grid. At any node the mean concentration of the variable
104 of interest was calculated within four local supports, each circular areas of radius 1000,
105 2000, 4000 and 8000 m. The ordinary least squares regression coefficient for the regression
106 of log-transformed mean concentration on log-transformed radius of the circular support
107 centered at \mathbf{x} provides an estimate of $\alpha(\mathbf{x}) - d$. Because d is a constant (2 in this case
108 with the analysis in two dimensions) the estimate of $\alpha(\mathbf{x})$ is easily obtained.

109 The ordinary least squares estimate of the regression coefficient must be treated
110 with some caution in these circumstances. This is because the circular supports are nested
111 within each other and so the residuals from the fitted line cannot be treated as independent.
112 However, we make no assumptions of independence in any subsequent inferences, and the
113 parametric bootstrapping of the background distribution of the index, described in section
114 2.1.3, explicitly reproduces this dependence.

115 For comparability we used the same radii for the four windows in all case studies.
116 In the first study (section 2.2 below) with the sparsest sampling the mean concentration
117 could not be evaluated at all nodes for the smallest radius, but checks showed that a value
118 could be obtained for all radii of 2000 m or more.

119 *2.1.2 Geostatistics.* To allow the bootstrapping of the distribution of the background
120 values of the singularity index we required a variogram function for the target variable.
121 This was computed for the variable after any transformation. Because the aim is to
122 obtain the variogram for the background process we wanted to minimize the effects of any

123 outlying observations, including spatial outliers which appear unusual only in their local
 124 context, since such values can have a disproportionate effect on estimates of the variogram
 125 (Lark, 2000). We therefore estimated the variogram using the standard estimator due to
 126 Matheron (1962), but also the alternative estimators due to Cressie and Hawkins (1980),
 127 Dowd (1984) and Genton (1998). Lark (2000) reviews these estimators and provides
 128 further detail. We applied them using the `georob` package for the R platform (Papritz,
 129 2016; R core team, 2014). Initially we estimated the variograms for different directions,
 130 but there was no marked anisotropy, particularly at lags corresponding to the scales at
 131 which the singularity index was computed, and so isotropic variograms were used.

132 Each variogram model was assessed by cross-validation. Each observation was re-
 133 moved from the data set in turn and predicted from the remaining ones by ordinary kriging.
 134 The standardized squared prediction error (SSPE) was computed for each cross-validation
 135 prediction:

$$\theta(\mathbf{x}) = \frac{\left\{ \tilde{Z}(\mathbf{x}) - z(\mathbf{x}) \right\}^2}{\sigma_{\text{OK}}^2(\mathbf{x})}, \quad (4)$$

136 where $\tilde{Z}(\mathbf{x})$ is the ordinary kriging prediction at location \mathbf{x} , $z(\mathbf{x})$ is the corresponding
 137 observed value and $\sigma_{\text{OK}}^2(\mathbf{x})$ is the corresponding ordinary kriging variance. The expected
 138 value of this statistic over all observations is one if the variogram model is correct, but
 139 outlying observations will affect both the numerator and denominator. We therefore ob-
 140 served the histograms of the cross-validation errors, and if the assumption that these were
 141 normal seemed plausible we examined the median value of the standardized squared pre-
 142 diction error. This should be close to 0.455 if the variogram model is correct, and will
 143 tend to be smaller if outliers are affecting the estimated variogram. On this basis one of
 144 the proposed variogram models was selected for further work.

145 *2.1.3 Mixture modelling and parametric bootstrapping.* The histograms of the singularity
 146 index values were examined. In all cases an assumption of a normal distribution with some
 147 additional mass in one or both tails seemed plausible, and so a mixture of normal distri-
 148 butions was fitted using the `mixtools` package in R, (Benaglia et al., 2009). The `boot.comp`

149 procedure in the package was applied to a simple random sample of 1000 observations to
150 evaluate the evidence that two or more components should be included in the model. This
151 procedure undertakes bootstrap resampling of the likelihood ratio statistic to evaluate the
152 evidence to include $p + 1$ rather than p component distributions for $p = 1, 2, \dots$. Once
153 the number of components had been selected a normal mixture model with this number
154 of constituent distributions was fitted with the `normalmixEM` procedure. This estimates p
155 sets of parameters (mean and standard deviation) and the proportions of each constituent
156 distribution: $\lambda_1, \dots, \lambda_{p-1}$. From these estimates one may compute the posterior density
157 for each component at any value of α . Lower and upper threshold values, α_L and α_U , were
158 identified to define the range of values of α to be identified with the background process.
159 The threshold values were those such that the posterior density of the component of the
160 mixture model identified with the background process was larger than that for any other
161 component for some α where $\alpha_L < \alpha < \alpha_U$.

162 The next question is how to identify which component of the mixture model rep-
163 resents the background. We would expect it to have a mean close to 2, and to be the
164 dominant component (largest value of λ). To support this inference, and to provide evi-
165 dence for the appropriateness of the mixture model approach to analysis of the singularity
166 index, we undertook a parametric bootstrap estimation of the parameters of the index
167 for a normal random variable (perhaps after transformation) with the same variogram
168 parameters as the data and the same spatial distribution. The process was as follows.

- 169 a. For the n data used in the computation of the observed values of the singularity
170 index, compute the distance matrix and from this the covariance matrix given the
171 estimated variogram parameters from the model selected by cross-validation.
- 172 b. Compute 1000 realizations of the normal variable with this covariance matrix, and the
173 mean of the (transformed) values of the original data using the `mvnorm` procedure
174 from the `MASS` package in R (Venables and Ripley, 2002).
- 175 c. For each realization in turn, back-transform the simulated values to the scale of the

176 original measurements.

177 d. Compute the singularity index from these data at the same grid locations as used in
178 the analysis of the real data, and with for the same set of windows.

179 e. Compute the mean and standard deviation of the singularity index of the simulated
180 data over all nodes and record these statistics.

181 f. Iterate steps (c)–(d) for each realization.

182 *2.2 Case study 1: Zn east of Dartmoor, south-west England*

183 This study area (see Figure 1) is a region within which anomalous concentrations
184 of soil zinc might be expected. This is because of the presence of stratiform sulphide
185 mineralizations in the region (Benham et al., 2005) which has a history of metal mining
186 from prior to the Roman occupation of Britain. Benham et al. (2005) report assessments
187 of geological information, geophysical surveys, information on known deposits and geo-
188 chemical data to support the expectation of such mineralizations. The latter data include
189 anomalous zinc concentrations in streambed sediment surveys and identification of zinc
190 enrichment in soils associated with magnetic anomalies identified by geophysical surveys.

191 The soil data from south-west England analysed in this paper were collected in
192 2013 according to the protocols of the Geochemical Baseline Survey of the Environment
193 (G-BASE) of the British Geological Survey (Johnson et al., 2005). The sample points
194 were located at more or less regular intervals, subject to constraints in the field, at a
195 density locally of about one sample per 8 km². Each sample was a composite formed from
196 cores collected at the centre and vertices of a 20-m square. The cores were length 15 cm
197 excluding surface litter. Material was subsequently air-dried, disaggregated and sieved to
198 pass 2 mm and sub-sampled by coning and quartering. A 50-g sub-sample was ground
199 in an agate planetary ball mill until 95% of the material was finer than 53 µm. Total
200 concentrations of each of some 50 elements were determined for each sample by X-Ray
201 Fluorescence Spectrometry.

202 *2.3 Case study 2: As in Counties Monaghan and Armagh, north of Ireland*

203 The Longford-Down terrane in the north-east of Ireland has a history of mineral
204 exploration; lead and zinc vein deposits have been worked since the nineteenth century. In
205 recent years the area has been recognised for its gold prospectivity. Dublin based junior
206 exploration company, Conroy Gold and Natural Resource, have defined a 30 mile gold
207 trend with a number of gold targets identified. These include the Clontibret gold target in
208 County Monaghan and additional targets that are identified along trend to the north east
209 at Clay Lake in County Armagh and to the south west in County Monaghan. The gold
210 mineralisation is associated with arsenopyrite and as such arsenic is used as a ‘pathfinder’
211 element for precious metal mineralisation. We therefore examined soil geochemical data
212 for anomalous As concentrations.

213 The soil data from Ireland analysed in this paper were collected in two surveys, the
214 Tellus survey of Northern Ireland and the Tellus Border survey of the six border counties
215 of the Republic of Ireland. The study area is shown in Figure 1. The geochemical survey
216 activities in these two projects are described by Young et al. (2016).

217 The sampling of soil in both Tellus and Tellus Border followed the field protocols of
218 G-BASE as described in section 2.2. In the Tellus survey soil sampling was undertaken
219 at a density of one sample per 2 km² and in Tellus Border at a density of one sample
220 per 3.6 km². Samples were dried and disaggregated by hand, then sieved to pass through
221 2 mm. The sub-2 mm fraction was milled using an agate planetary ball mill to produce
222 a sample of predominantly < 53 µm fraction. A 1-g sub-sample of the milled material
223 was treated by two-acid (ratio of 2:1 HNO₃:HCl *aqua regia* variant) sample digestion,
224 and the digestate was analysed for concentrations of a range of elements including As by
225 multi-element ICP-MS analysis (Knights, 2013).

226 *2.4 Case study 3: Pb in the Trent valley, East Midlands of England*

227 This study area (Figure 1) comprises land primarily in rural environments around
228 the River Trent in the East Midlands of England, although the urban centres of Worksop

229 and Doncaster lie respectively on the southern and northern corners of its western edge.
230 It was selected for examination for anomalies in soil lead concentration. The area does
231 not include any known geogenic sources of lead, being some way to the east of the nearest
232 mineralization domains for this element (Ander et al. 2013). It does not include a major
233 urbanised domain for lead, as identified by Ander et al. (2013) but anthropogenic sources
234 of lead from industrial activity, paint, leaded petrol and other sources are possible in the
235 west due to the populated areas of Worksop and Doncaster and associated small towns.
236 A priori, a likely source of lead is the alluvium of the River Trent. It is known that the
237 Trent alluvium may have instances of large concentrations of lead (Izquierdo et al., 2014).
238 Isotopic studies of this lead (Izquierdo et al., 2014) show that it has multiple sources
239 including geogenic ones — lead mineralization in the Peak District of Derbyshire in the
240 East Midlands of England upstream and to the west of the selected study area. This
241 region includes deposits of lead which have been mined since the Roman occupation, and
242 are also subject to natural weathering. Lead also occurs in East Midlands coal deposits.
243 There is also evidence for anthropogenic lead, at least some of which can be attributed to
244 lead tetraethyl which was used as an additive in petrol in the United Kingdom until 1999,
245 although the lead content of petrol in the UK was reduced from 1986 (Noble et al., 2008).
246 Geogenic sources of lead contribute to alluvium through weathering and transport by
247 water. The anthropogenic sources of lead contribute through discharge of wastes directly
248 into rivers and onto soils.

249 The soil data used for this case study were collected as part of the G-BASE pro-
250 gramme following the same protocols as described for the Zn data in section 2.2, but with
251 sampling at a density of approximately one sample per 2 km² with samples located as
252 close as possible to the centres of alternate 1-km² cells of the British National Grid.

253 *2.5 Case study 4: Hf in north Norfolk, eastern England*

254 This study area is in the north of Norfolk in eastern England (Figure 1). The
255 element considered here is hafnium (Hf). This element is known to be relatively enriched

256 (along with zirconium) in aeolian deposits (Taylor et al., 1983), and this association has
257 been confirmed for the loess deposits and coversands of eastern England by Scheib and
258 Lee (2010). These aeolian deposits are of late Pleistocene origin when the southern limit
259 of the British ice sheet was just to the north of the study area. Loess is found in the
260 north-eastern part of the selected area and coversands in the south-west.

261 The soil data used in this case study were collected according to the same field and
262 analytical protocols as the lead data described in section 2.4, with sampling at a mean
263 density of one sample per 2 km².

264 **3. Results**

265 *3.2 Case study 1: Zn east of Dartmoor, south-west England*

266 On the original scale of measurement (mg kg⁻¹) the data on Zn concentration are
267 somewhat skew (Figure 2, Table 1) but this is reduced by transformation to logarithms.
268 Most of the larger concentrations are in the east of the region in soil formed over sand-
269 stones, mudstones, metasandstones, metamudstones and slates, the latter formed by meta-
270 morphosis under the influence of the igneous granite intrusion in the east of the region
271 which underlies Dartmoor (British Geological Survey, 1995).

272 There are some differences among the empirical variograms obtained with different
273 estimators (Figure 4). The histograms of the cross-validation errors suggest that these may
274 be assumed to be normal (Figure 5) and the median SSPE (Table 2) for the variogram
275 fitted to estimates obtained by the robust estimator of Cressie and Hawkins (1980) is
276 closest to the expected value of 0.455, so this was used for the parametric bootstrapping
277 of the singularity index for the background random variable (Table 3).

278 Table 4 shows that the two-component mixture model was favoured for the values
279 of the singularity index for the Zn data. The dominant component has a standard de-
280 viation of 0.304, which is close to the median value of the standard deviation over the
281 1000 parametric bootstrap resamples (Table 3) and within the interquartile range. This
282 supports the interpretation of the mixture model as showing, in the dominant component,

283 the singularity index values for the background process, with additional mass in the tails
284 of the distribution, corresponding to anomalies, introduced by a minor component with a
285 larger standard deviation (Figure 6). The posterior likelihood of this second component is
286 larger for values of the singularity index smaller than 1.51 and larger than 2.85, so these
287 values were used as thresholds (Figure 7).

288 Most of the enrichment anomalies in Figure 7 appear in the east of the region.
289 Note in particular that there are three clusters which lie on a line approximately north
290 north-east to south south west, aligned with the distribution of known sites with stratified
291 mineralization in the area. This suggests that the geochemical anomalies identified by the
292 analysis are, at least in part, the result of local mineralization, some of which may be of
293 economic significance.

294 *3.3 Case study 2: As in Counties Monaghan and Armagh, north of Ireland*

295 The original data on As were markedly skew (Figure 8, Table 1) and this was reduced
296 by transformation to logarithms although the histograms suggest that a contaminated
297 normal model may be appropriate with additional observations in an upper tail. There
298 are marked differences between the variograms estimated by different methods (Figure
299 10). The cross validation errors in Figure 11 suggest that a normal model of these is
300 plausible. The median SSPE for the variogram model fitted to estimates obtained with
301 the estimator proposed by Dowd (1984) is 0.41, closer to 0.455 than that for any other
302 model. This was used to obtain the parametric bootstrap samples of the statistics for the
303 singularity index in Table 3.

304 Table 4 shows that a two-component mixture model was favoured for the singularity
305 index. The dominant component had a standard deviation of 0.182. This was somewhat
306 smaller than the median value of the parametric bootstrap resamples of the singularity
307 index (Table 3) and outside the 95 percentile range (0.193–0.280). On the assumption that
308 the dominant component represents the background process the thresholds for anomalies
309 are 1.67 and 2.54 (Figure 13).

310 The arsenic enrichment anomalies evident in Figure 13 correspond to known arsenic
311 (and gold) mineralisation identified through mineral exploration in the area. Both oc-
312 cur as coincident discrete packages along the line of the Orlock Bridge Fault, which is
313 believed to be a controlling feature. The anomaly at location 270 500E (Irish National
314 Grid, ING), 327 000N(ING) (County Monaghan) is located on the northern edge of the
315 previously-identified gold anomaly at the Glenish gold target. The Clay Lake target at
316 282 000E(ING), 335 100N(ING) shows good correlation with the singularity anomaly in
317 that location. However of particular interest, the Clontibret gold deposit at location
318 275 800E(ING), 330 000N(ING) shows no corresponding singularity anomaly in the soil
319 dataset, based on the thresholds used. A minor anomaly is evident along strike between
320 Glenish and Clay Lake which sits in the general gold trend identified. A further anomaly
321 is located along trend to the south west at 257000E(ING), 311000N(ING) which may be
322 related to the same mineralisation event. This anomaly at 257 000E(ING), 311 000N(ING)
323 is located to the south of the mapped location of the Orlock Bridge Fault, rather than to
324 the north as is the case at Glenish and Clay Lake.

325 In addition to the major NE - SW basement orientation, structural mapping in the
326 area has identified NNE and NW trending lineaments and faults. Further anomalies in the
327 area could be interpreted to follow the discrete package style of occurrence which typifies
328 the mineralisation along the Orlock Bridge fault, in these other orientations.

329 *3.4 Case study 3: Pb in the Trent valley, East Midlands of England*

330 The original data on lead concentrations were very strongly skewed (Figure 14, Table
331 1) and this was reduced by log transformation although the coefficient of skewness for the
332 transformed data still exceeds 1. There are marked differences between the variograms
333 estimated by different methods (Figure 16) and the median SSPE for the variogram model
334 fitted to estimates obtained with the estimator proposed by Dowd (1984) is 0.46, which
335 is very close to the expectation for normal kriging errors with a correct variogram model.
336 This mode was used to obtain the parametric bootstrap samples of the statistics for the

337 singularity index in Table 3.

338 The two-component mixture model was favoured for the singularity index (Table 4,
339 Figure 18). The standard deviation of the dominant component was 0.140, which is just
340 outside the 95 percentile range for the bootstrap resampled estimate of this statistic under
341 the lognormal model (0.11–0.13). Under the two component mixture model the minor com-
342 ponent has a mean somewhat less than 2.0 (1.85) and so introduces most additional mass
343 into the lower tail, corresponding to enrichment anomalies. The thresholds for anomalies
344 under the mixture model were 1.81 and 2.52.

345 Figure 19 shows the singularity index and the thresholded values. It is clear that
346 much of the region corresponding to enrichment anomalies is close to the course of the
347 River Trent, shown by a white line in Figure 19b. There are also other patches with
348 enrichment anomalies, notably to the west of the river. The largest such patch is near
349 the British National Grid coordinates 470 000E, 381 000N. This corresponds to the small
350 town of Retford in Nottinghamshire. While this town does not have a heritage of heavy
351 industry it is a significant point of convergence for transport routes with two railway lines,
352 significant trunk roads and a canal historically used for transport of industrial goods.
353 The River Idle also passes through the town. This river, a tributary of the Trent, has
354 a low water quality rating due to the urban setting of its tributaries and its reception
355 of significant discharges from sewage treatment works (Environment Agency, 2006). In
356 summary, much of the spatial distribution of enrichment anomalies is accounted for by
357 the course of the Trent, and other enrichment anomalies are likely, as with the patch near
358 Retford, to reflect anthropogenic factors.

359 *3.5 Case study 4: Hf in north Norfolk, eastern England*

360 The data on hafnium concentrations on the original scale are mildly skewed (Table
361 1, Figure 20) and have a marked negative skew on the logarithmic scale. For this reason
362 a transformation to square roots was used. The larger Hf concentrations are seen in the
363 north east and south west of the region (Figure 21) corresponding to known loess and

364 cover sand deposits respectively. There are differences between the variogram estimates
365 obtained with different estimators (Figure 22) and the cross validation supports the use
366 of the model fitted to estimates obtained with the estimator proposed by Dowd (1984).

367 A two-component mixture model was favoured (Table 4). The dominant component
368 has a standard deviation of 0.082 which is close to the median value for the parametric
369 bootstrap resample estimates (0.087) and is within the 95 percentile range (0.076–0.101).
370 The mixture model introduces very little additional mass from the second component,
371 for which $\lambda = 0.03$. The threshold values for identification of anomalies according to the
372 mixture model are 1.69 and 2.24. Very few values fall outside these limits, as can be seen
373 in Figure 25. This suggests that, while there are areas with larger concentrations of Hf
374 than others, and these can be explained from the known distribution of aeolian deposits,
375 this spatial variation is consistent with the (trans) normal distribution and there is no
376 evidence for substantial local enrichment or depletion inconsistent with this background
377 variation.

378 4. Discussion and Conclusions

379 In this study we examined data on concentrations of four elements in the soil in
380 four contrasting settings. In three of these cases there was clear evidence for geochemical
381 anomalies, predominantly enrichment. In these cases the pattern of anomalies was consis-
382 tent with independent knowledge about sources, geogenic or anthropogenic, of enrichment
383 — the stratiform mineralizations near Dartmoor, the geogenic gold/arsenic mineral oc-
384 currences in the Longford-Down terrane, the Trent alluvium and anthropogenic sources
385 of lead in the East Midlands of England. There was no substantial evidence of anomalies
386 in the data on Hf in north Norfolk. While elevated values were indeed found as expected
387 in areas with known aeolian deposits, these are consistent with a simple (trans)normal
388 process, with no evidence of locally anomalous behaviour at the scales examined.

389 In all cases the likelihood ratio tests favoured a mixture of normals model with two
390 but no more components. In all the minor component (smaller λ) had the larger standard

391 deviation and so introduced additional mass into both tails of the overall distribution,
392 although in most cases this was not symmetrical, and in the case of lead in the East
393 Midlands of England the mean of the minor component was markedly smaller than 2.0,
394 accounting for a marked lower tail in the overall distribution of the singularity index. The
395 double-log plots of the empirical survival function of α for each case study (Figure 26) do
396 not, in any of the cases, clearly comprise linear segments. This suggests that the mixture
397 model used here is a more suitable way to determine threshold values of the singularity
398 index.

399 In the case of Zn and Hf the standard deviation of the major component in the
400 mixture model fell within the 95 percentile range of the parametric bootstrapped values
401 extracted from values simulated with the selected variogram. In the case of Pb and As the
402 standard deviation fell just outside this range, but was much closer to the bootstrapped
403 values than was the standard deviation for the minor component. This supports the
404 mixture interpretation of the singularity index values, and the thresholds derived from
405 this. It is possible that the differences reflect limitation of the robust estimation of the
406 variogram. It may also be that, while the assumption of normality for the transformed
407 data seemed reasonable, as judged by the histograms, there may be structure in the spatial
408 variation with non-normal higher-order moments — features which require multiple-point
409 geostatistics (Meerschman et al., 2013).

410 It is notable that the two-component mixture model for the singularity index is com-
411 patible with a wide range of behaviours by the variable of interest. The mass introduced
412 into the tails of the distribution may be very small in both tails if the standard deviation
413 of the minor (non-background) component is not much larger than the standard deviation
414 of the major component. That was seen in the case of hafnium in this study. With a
415 larger standard deviation for the minor component, more mass can be introduced into
416 both tails, modelling the presence of both enrichment and depletion anomalies. A strong
417 preponderance of enrichment anomalies can be modelled if the mean for the minor compo-

418 nent in the model is markedly smaller than two (as with lead). In a case where there was
419 a combination of locally intensive enrichment (e.g. from industrial contamination) and
420 more diffuse enrichment by processes such as wind dispersal, this might be represented by
421 a minor component in the mixture model with a large standard deviation creating a heavy
422 lower tail for the overall distribution of the singularity index, although in some cases more
423 than two components might be required in the mixture model.

424 If the mean of the background process is not stationary (e.g. there is a spatial
425 trend) then this should not markedly affect the corresponding component of the distri-
426 bution model for the singularity index as this depends on the local variability in much
427 the same way that ordinary kriging is robust to trends (Goovaerts, 1997). However, if
428 the background process is not stationary in the variance and autocorrelation, then a more
429 complex model would be necessary, and this is a topic for further study. Note that if there
430 was non-stationarity in the variance then the median value of SSPE, examined in the
431 cross-validation of the variogram models (Table 2) would be expected to deviate markedly
432 from 0.45 (Lark, 2009).

433 To conclude, it has been shown that anomalous values (or their absence) can be
434 identified in soil geochemical data by means of the singularity index, and that the inter-
435 pretation of this index can be facilitated with a mixture model. More work is needed on the
436 statistics of the index, particularly for the robust characterization of the background dis-
437 tribution under a null (trans)normal distribution, and for the modelling of non-stationary
438 background processes.

439 **5. Acknowledgements**

440 MP and DMR were funded by the Geological Survey of Ireland under Short Call
441 project ‘Geochemical anomaly detection: spatial analysis for improved use of geochemical
442 data’, reference 2015-sc-069. We are grateful to Fiona McEvoy, Paul Lusty, Chris Yeomans
443 and Gerry Stanley for helpful discussions. This paper is published with the permission of
444 the Executive Director of the British Geological Survey (NERC).

445 **References**

- 446 Agterberg, F.P. 2012. Multifractals and geostatistics. *Journal of Geochemical Exploration*, 122, 113–122.
- 447
- 448 Allègre, C.J., Lewin, E. 1995. Scaling laws and geochemical distributions. *Earth and Planetary Science Letters*. 132, 1–13.
- 449
- 450 Ander, E.L., Johnson, C.C., Cave, M.R., Palumbo-Roe, B., Nathanail, C.P., Lark, R.M.
- 451 2013. Methodology for the determination of normal background concentrations of
- 452 contaminants in English soil. *Science of the Total Environment*, 454–455, 604–618.
- 453 Benaglia, T., Chauveau, D., Hunter, D.R., Young, D. 2009. mixtools: An R Package for
- 454 Analyzing Finite Mixture Models. *Journal of Statistical Software*, 32, 1–29.
- 455 Benham, A.J., McEvoy, F.M., Rollin, K.E. 2005 Potential for stratiform massive sulphide
- 456 mineralisation in south-west England. *Transactions of the Institution of Mining and Metallurgy, Section B Applied Earth Science*. 113, 227–246.
- 457
- 458 Breward, N., 2007. Arsenic and presumed resistate trace element geochemistry of the
- 459 Lincolnshire (UK) sedimentary ironstones and revealed by a regional geochemical
- 460 survey using soil, water and stream sediment sampling. *Applied Geochemistry*, 22,
- 461 1970–1993.
- 462 British Geological Survey. 1995. Dartmoor Forest. Solid and Drift Map. 1:63,360/1:50,000
- 463 geological map series, New Series Sheet 338. British Geological Survey, Keyworth,
- 464 Nottingham.
- 465 Chen, Z., Cheng, Q., Chen, J., Xie, S. 2007. A novel iterative approach for mapping
- 466 local singularities from geochemical data. *Nonlinear Processes in Geophysics*, 14,
- 467 317–324.
- 468 Cheng, Q. 2007. Mapping singularities with stream sediment geochemical data for pre-
- 469 diction of undiscovered mineral deposits in Gejiu, Yunnan Province, China. *Ore*

470 Geology Reviews, 32, 314–324.

471 Cheng, Q. 2012. Singularity theory and methods for mapping geochemical anomalies
472 caused by buried sources and for predicting undiscovered mineral deposits in covered
473 areas. *Journal of Geochemical Exploration*, 122, 55–70.

474 Cressie, N., Hawkins, D. 1980. Robust estimation of the variogram. *Journal of the*
475 *International Association of Mathematical Geology* 12, 115–125.

476 Dowd, P.A. 1984. The variogram and kriging: robust and resistant estimators. In:
477 *Geostatistics for Natural Resources Characterization* (eds G. Verly, M. David, A.G.
478 Journel and A. Marechal), Part 1. pp. 91–106. D. Reidel, Dordrecht.

479 Environment Agency 2006. *The Idle and Torne Catchment Abstraction Management*
480 *Strategy*. Environment Agency, Bristol.

481 Genton, M.G. 1998. Highly robust variogram estimation. *Mathematical Geology* 30,
482 213–221.

483 Goovaerts, P. 1997. *Geostatistics for Natural Resources Evaluation*. Oxford University
484 Press, New York.

485 Izquierdo, M., Tye, A.M., Chenery, S.R. 2012. Sources, lability and solubility of Pb in
486 alluvial soils of the River Trent catchment, U.K. *Science of the Total Environment*,
487 433, 110–122.

488 Johnson, C.C., Breward, N., Ander, E. L., Ault, L. 2005. G-BASE: Baseline geochem-
489 ical mapping of Great Britain and Northern Ireland. *Geochemistry: Exploration,*
490 *Environment, Analysis* 5, 1–13.

491 Knights, K.V. 2013. Quality control and statistical summaries of Tellus Border topsoil
492 regional geochemical data. Report Version 1.0. Geological Survey of Ireland and
493 Geological Survey of Northern Ireland joint report.

- 494 Lark, R.M. 2000. A comparison of some robust estimators of the variogram for use in
495 soil survey. *European Journal of Soil Science* 51, 137–157.
- 496 Lark, R.M. 2009. Kriging a soil variable with a simple non-stationary variance model.
497 *Journal of Agricultural Biological and Environmental Statistics*, 14, 301–321.
- 498 Lark, R.M., Ander, E.L., Cave, M.R., Knights, K.V., Glennon, M.M, Scanlon, R.P. 2014.
499 Mapping trace element deficiency by cokriging from regional geochemical soil data:
500 a case study on cobalt for grazing sheep in Ireland. *Geoderma*, 226–227, 64–78.
- 501 Lin, Y., Cheng, B., Shyu, G., Chang, T. 2010. Combining a finite mixture distribution
502 model with indicator kriging to delineate and map the spatial patterns of soil heavy
503 metal pollution in Chunghua County, central Taiwan. *Environmental Pollution*, 158,
504 235–244.
- 505 Liu, Y., Cheng, Q., Xia, Q., Wang, X. 2014. Identification of REE mineralization-related
506 geochemical anomalies using fractal/multifractal methods in the Nanling belt, South
507 China. *Environmental Earth Sciences*, 72, 5159–5169.
- 508 Matheron, G. 1962. *Traité de Géostatistique Appliqué, Tome 1. Mémoires du Bureau*
509 *de Recherches Géologiques et Minières, Paris.*
- 510 Meerschman, E., Van Meirvenne, M., Van De Vijver, E., De Smedt, T.,Islam, M.M., Saey,
511 T. 2013. Mapping complex soil patterns with multiple-point geostatistics. *European*
512 *Journal of Soil Science*, 64, 183–191.
- 513 Noble, S.R., Horstwood, M.S.A., Davy, P., Pashley, V., Sprio, B., Smith, S. 2008.
514 Evolving Pb isotope signatures of London airborne particulate matter (PM₁₀) —
515 constraints from on-filter and solution-mode MC-ICP-MS. *Journal of Environmental*
516 *Monitoring*, 10, 830–836.
- 517 Papritz, A. 2016. *georob: Robust Geostatistical Analysis of Spatial Data. R package*
518 *version 0.2-3. <http://CRAN.R-project.org/package=georob>*

519 R Core Team 2014. R: A language and environment for statistical computing. R Founda-
520 tion for Statistical Computing, Vienna, Austria. URL <http://www.R-project.org/>.

521 Rawlins, B.G., Lark, R.M., Webster, R., O'Donnell, K.E. 2006. The use of soil survey
522 data to determine the magnitude and extent of historic metal deposition related
523 to atmospheric smelter emissions across Humberside, UK. *Environmental Pollution*,
524 143, 416–426.

525 Scheib, A.J., Lee, J.R. 2010. The application of regional-scale geochemical data in defin-
526 ing the extent of aeolian sediments : the Late Pleistocene loess and coversand de-
527 posits of East Anglia, UK. *Quaternary newsletter*, 120, 5–14.

528 Taylor, S.R., McLennan, S.M., McCulloch, M.T. 1983. Geochemistry of loess, continental
529 crustal composition and crustal model ages. *Geochimica et Cosmochimica Acta*, 47,
530 1897–1905.

531 Venables, W. N., Ripley, B. D. 2002. *Modern Applied Statistics with S*. Fourth Edition.
532 Springer, New York.

533 Young, M.E., Knights, K.V., Smyth, D., Glennon, M.M., Scanlon, R.P., Gallagher, V.
534 2016. The Tellus geochemical surveys, results and applications. In *Unearthed*,
535 impacts of the Tellus surveys of the north of Ireland. (ed. M.E. Young), pp 33–
536 52. Royal Irish Academy, Dublin.

Table 1: Summary statistics for soil variables on original and transformed scale

Variable	Mean	Median	Standard deviation	Skewness	Quartile 1	Quartile 3
Zn mg kg ⁻¹	96.64	78.05	77.70	3.35	45.42	126.93
Zn log (mg kg ⁻¹)	4.34	4.36	0.68	0.07	3.82	4.84
As mg kg ⁻¹	8.00	5.76	9.48	6.58	3.91	8.53
As log (mg kg ⁻¹)	1.79	1.75	0.71	0.42	1.36	2.14
Pb mg kg ⁻¹	49.52	35	62.98	11.16	28	49
Pb log (mg kg ⁻¹)	3.68	3.56	0.56	1.44	3.33	3.89
Hf (mg kg ⁻¹)	7.59	7.3	2.37	1.40	6.1	8.6
Hf (mg kg ⁻¹) ^{0.5}	2.72	2.70	0.41	0.46	2.47	2.93

Table 2: Mean and median standardized squared prediction error for cross-validation on each variable

Variable	Standardized squared prediction error							
	Variogram estimator							
	Matheron		Cressie– Hawkins		Dowd		Genton	
	Mean	Median	Mean	Median	Mean	Median	Mean	Median
Zn $\log(\text{mg kg}^{-1})$	0.90	0.32	1.27	0.43	1.71	0.51	1.17	0.39
As $\log(\text{mg kg}^{-1})$	0.86	0.25	1.09	0.33	1.35	0.41	1.13	0.34
Pb $\log(\text{mg kg}^{-1})$	1.02	0.23	1.58	0.34	2.15	0.46	1.71	0.37
Hf $(\text{mg kg}^{-1})^{0.5}$	0.96	0.29	1.19	0.37	1.35	0.43	4.25	1.31

Table 3: Mean and quantiles of parameters of the parametric-bootstrapped singularity index under the (log)normal null model

Quantile	Mean of α					Standard deviation of α				
	0.025	0.25	0.50	0.75	0.975	0.025	0.25	0.50	0.75	0.975
Variable										
Zn log (mg kg ⁻¹)	2.02	2.05	2.08	2.10	2.17	0.235	0.272	0.298	0.331	0.413
As log (mg kg ⁻¹)	2.03	2.05	2.06	2.07	2.09	0.193	0.216	0.228	0.243	0.280
Pb log (mg kg ⁻¹)	2.010	2.015	2.018	2.022	2.030	0.109	0.117	0.121	0.125	0.134
Hf (mg kg ⁻¹) ^{0.5}	2.002	2.007	2.009	2.011	2.016	0.076	0.083	0.087	0.0912	0.101

Table 4: Mixture fitting for singularity index

Variable	Log-likelihood ratio and P -values				Mixture-model parameters					
	2 components		3 components		Component 1			Component 2		
	L	P	L	P	λ	μ	σ	λ	μ	σ
Zn log (mg kg ⁻¹)	17.56	0.010	9.65	0.1	0.73	2.12	0.304	0.27	2.03	0.487
As log (mg kg ⁻¹)	39.59	<0.001	5.05	0.28	0.81	2.08	0.182	0.19	2.00	0.364
Pb log (mg kg ⁻¹)	104.05	<0.001	6.78	0.16	0.81	2.10	0.140	0.19	1.85	0.319
Hf (mg kg ⁻¹) ^{0.5}	13.38	0.04	4.68	0.30	0.97	2.01	0.082	0.03	2.11	0.157

Figure captions

Figure 1. Map of the United Kingdom and Ireland showing the locations of the rectangular regions within which the singularity index was evaluated for some element in the topsoil. a). East of Dartmoor in the south-west of England (Zn); b). Longford-Down terrane in Counties Monaghan and Armagh in the north of Ireland (As); c). Part of the Trent valley in the East Midlands of England (Pb) d). Part of North Norfolk in eastern England (Hf).

Figure 2. Boxplots and histograms for (2a and 2b) soil Zn content from the south-west study area and (2c and 2d) soil Zn content transformed to natural logarithms.

Figure 3. Post-plot of the Zn data, the symbols distinguish sample points in the quartiles of the distribution. Coordinates are in metres relative to the origin of the British National Grid.

Figure 4. Empirical variograms for Zn content from the south-west study area with fitted models. Estimators are Matheron (4a), Cressie-Hawkins (4b), Dowd (4c) and Genton (4d).

Figure 5. Histograms of cross-validation errors for Zn content from the south-west study area. Estimators are Matheron (5a), Cressie-Hawkins (5b), Dowd (5c) and Genton (5d).

Figure 6. Histogram of the singularity index for Zn content from the south-west study area with PDFs for two components of the mixture superimposed.

Figure 7. (Top) values of the singularity index for Zn and (bottom) values thresholded on the basis of the mixture model: enrichment anomaly in black, background in grey, depletion anomaly hachured. The dark grey symbols indicate the locations of known stratiform mineral deposits in the area, the grey star indicating a deposit where Zn is a major ore element. Coordinates are in metres relative to the origin of the British National Grid.

Figure 8. Boxplots and histograms for (8a and 8b) soil As content from the Longford-Down terrane and (8c and 8d) soil As content transformed to natural logarithms.

Figure 9. Post-plot of the As data, the symbols distinguish sample points in the quartiles of the distribution. Coordinates are in metres relative to the origin of the Irish National Grid.

Figure 10. Empirical variograms for soil As content from the Longford-Down terrane with fitted models. Estimators are Matheron (10a), Cressie-Hawkins (10b), Dowd (10c) and Genton (10d).

Figure 11. Histograms of cross-validation errors for soil As content from the Longford-Down study area. Estimators are Matheron (11a), Cressie-Hawkins (11b), Dowd (11c) and Genton (11d).

Figure 12. Histogram of the singularity index for soil As content from the Longford-Down study area with PDFs for two components of the mixture superimposed.

Figure 13. (Top) values of the singularity index for As and (bottom) values thresholded on the basis of the mixture model: enrichment anomaly in black, background in grey, depletion anomaly hachured. Coordinates are in metres relative to the origin of the Irish National Grid.

Figure 14. Boxplots and histograms for (14a and 14b) soil Pb content from the East Midlands study area and (14c and 14d) soil Pb content transformed to natural logarithms.

Figure 15. Post-plot of the Pb data, the symbols distinguish sample points in the quartiles of the distribution. Coordinates are in metres relative to the origin of the British National Grid.

Figure 16. Empirical variograms for soil Pb content from the East Midlands study area with fitted models. Estimators are Matheron (16a), Cressie-Hawkins 16b), Dowd

(16c) and Genton (16d).

Figure 17. Histograms of cross-validation errors for soil Pb content from the East Midlands study area. Estimators are Matheron (17a), Cressie-Hawkins (17b), Dowd (17c) and Genton (17d).

Figure 18. Histogram of the singularity index for soil Pb content from the East Midlands study area with PDFs for two components of the mixture superimposed.

Figure 19. (Top) values of the singularity index for Pb and (bottom) values thresholded on the basis of the mixture model: enrichment anomaly in black, background in grey, depletion anomaly hachured. The white line shows the course of the River Trent. Coordinates are in metres relative to the origin of the British National Grid.

Figure 20. Boxplots and histograms for (20a and 20b) soil Hf content from the North Norfolk study area and (20c and 20d) soil Hf content transformed to natural logarithms.

Figure 21. Post-plot of the Hf data, the symbols distinguish sample points in the quartiles of the distribution. Coordinates are in metres relative to the origin of the British National Grid.

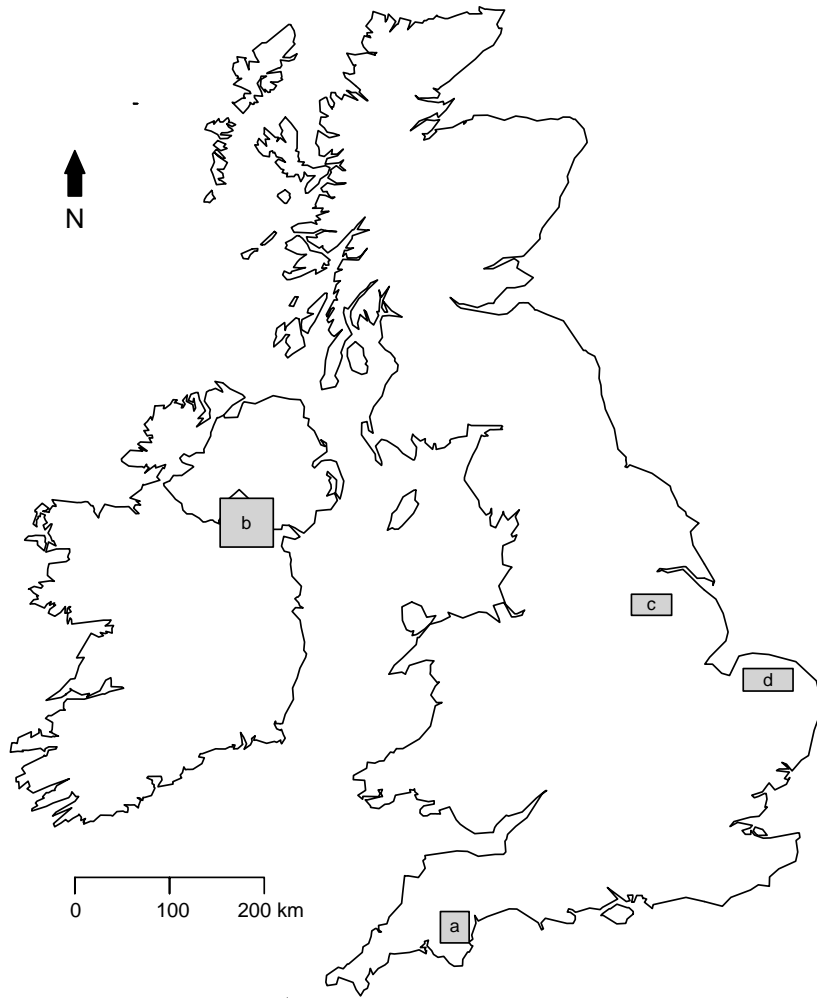
Figure 22. Empirical variograms for soil Hf content from the North Norfolk study area with fitted models. Estimators are Matheron (22a), Cressie-Hawkins (22b), Dowd (22c) and Genton (22d).

Figure 23. Histograms of cross-validation errors for soil Hf content from the North Norfolk study area. Estimators are Matheron (23a), Cressie-Hawkins (23b), Dowd (23c) and Genton (23d).

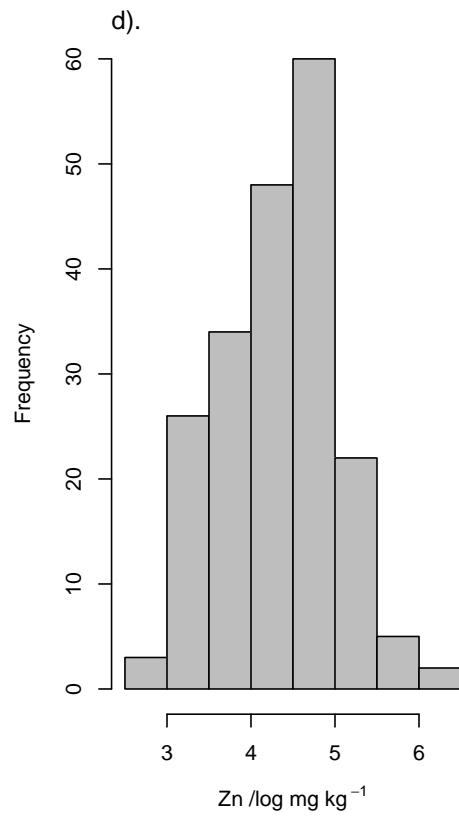
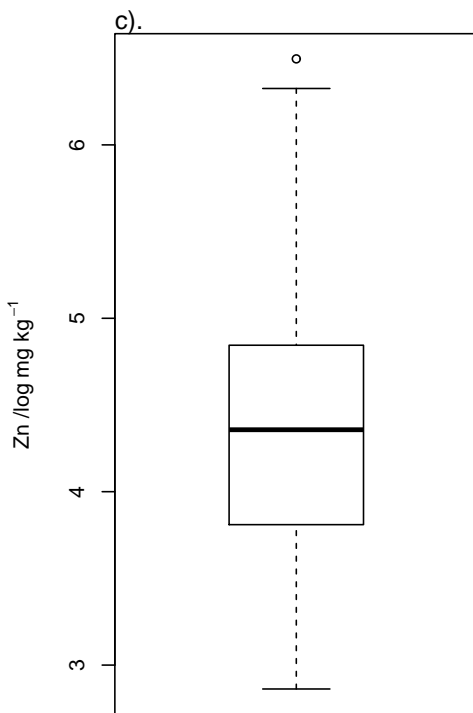
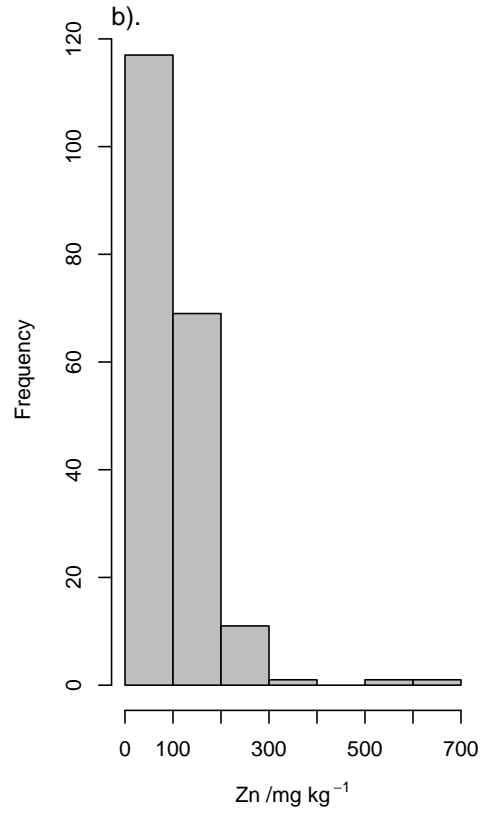
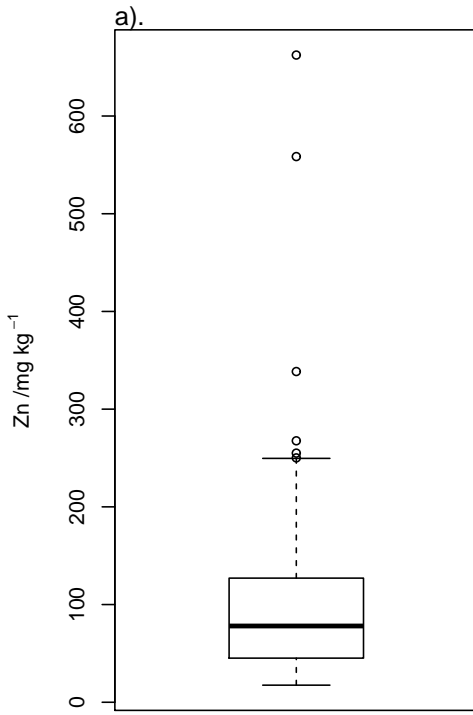
Figure 24. Histogram of the singularity index for soil Hf content from the North Norfolk study area with PDFs for two components of the mixture superimposed.

Figure 25. (Top) values of the singularity index for Hf and (bottom) values thresholded on the basis of the mixture model: enrichment anomaly in black, background in grey, depletion anomaly hachured. Coordinates are in metres relative to the origin of the British National Grid.

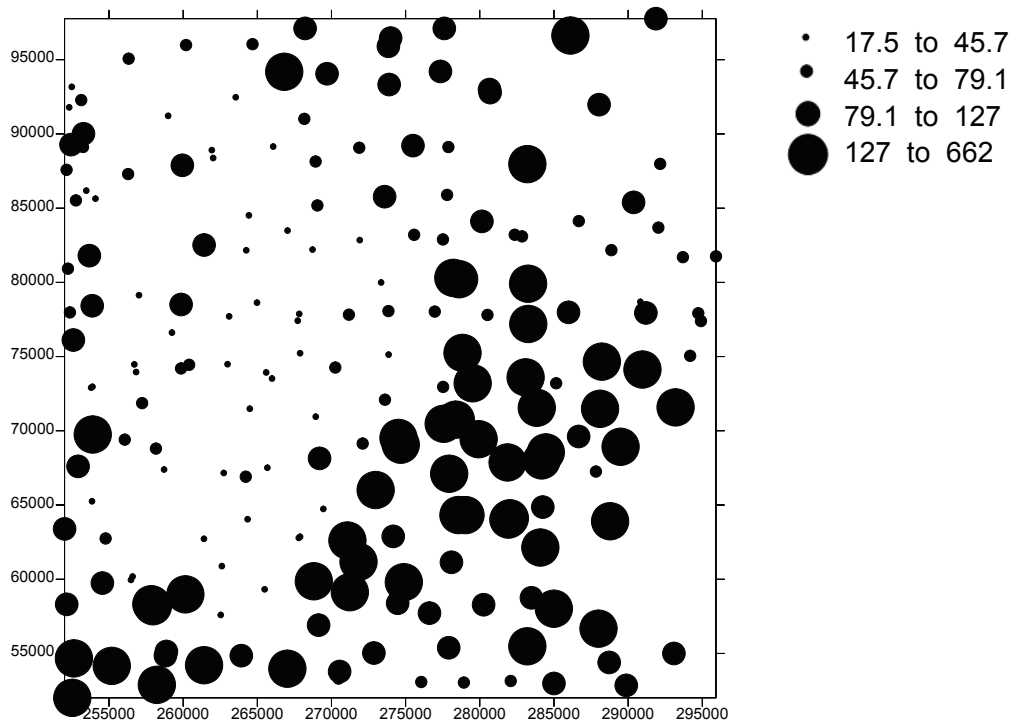
Figure 26. Plots of the empirical survival function of the singularity index, i.e. the area corresponding to values of the index less than α on double-log axes for a) Zn in the south-west study area; b) As at Longford-Down; c) Pb in the East Midlands and d) Hf in North Norfolk.



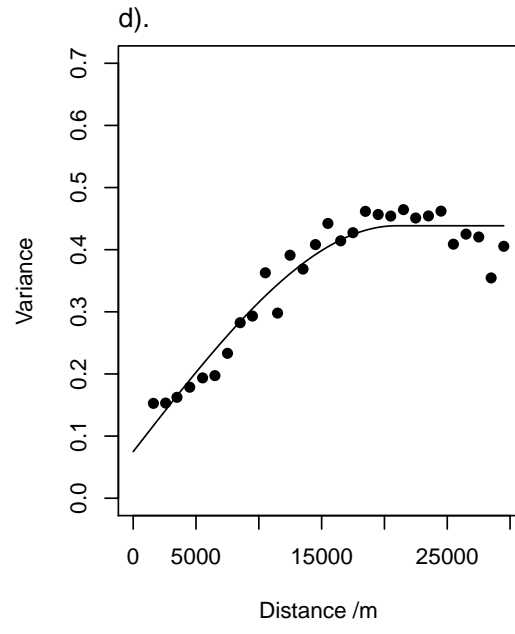
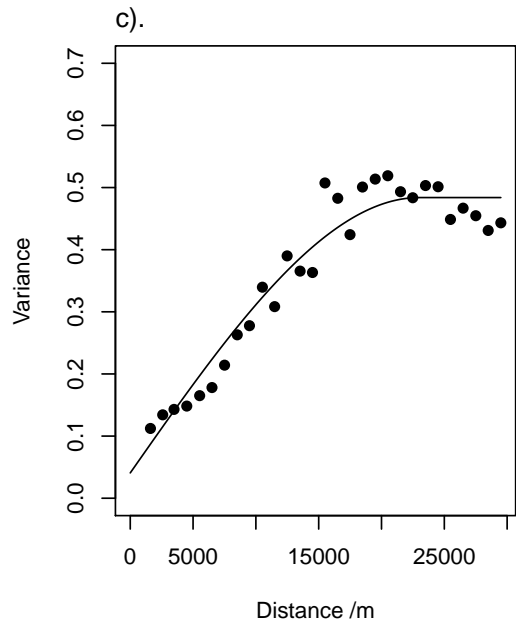
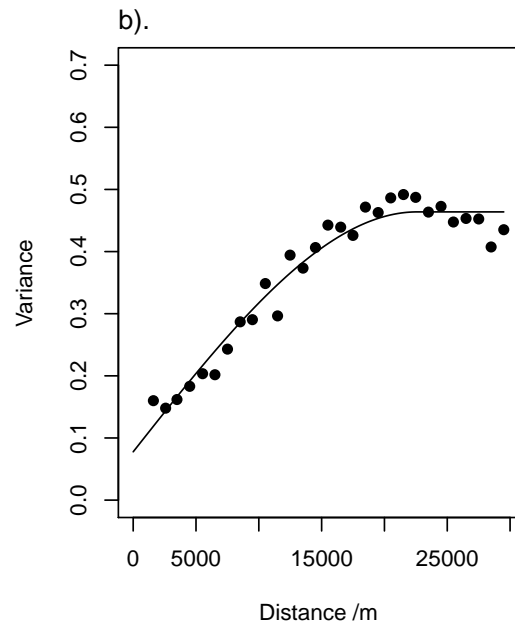
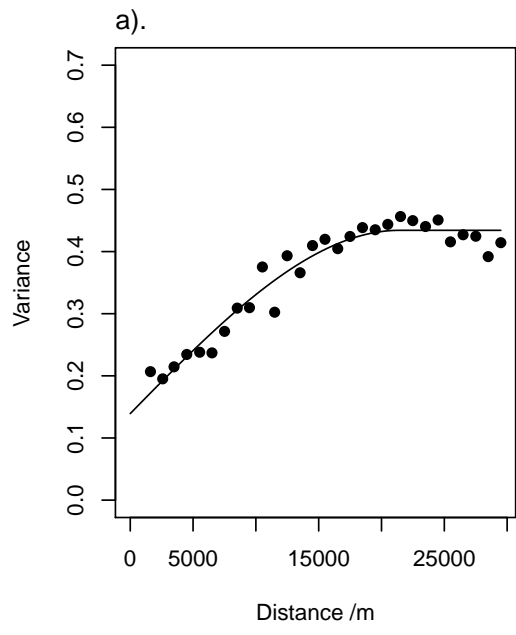
1: Fig 1



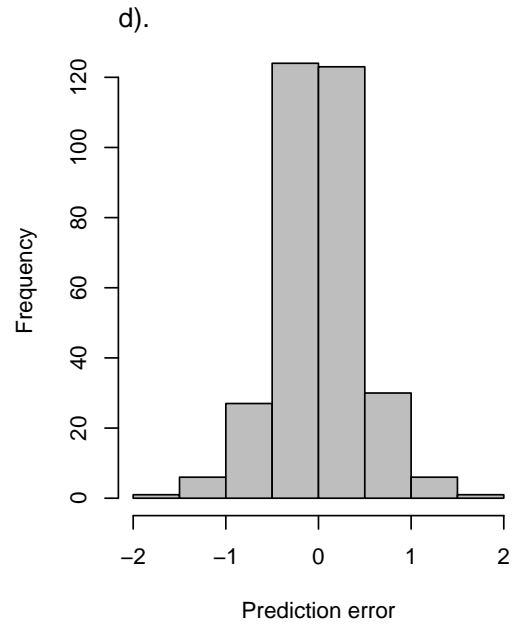
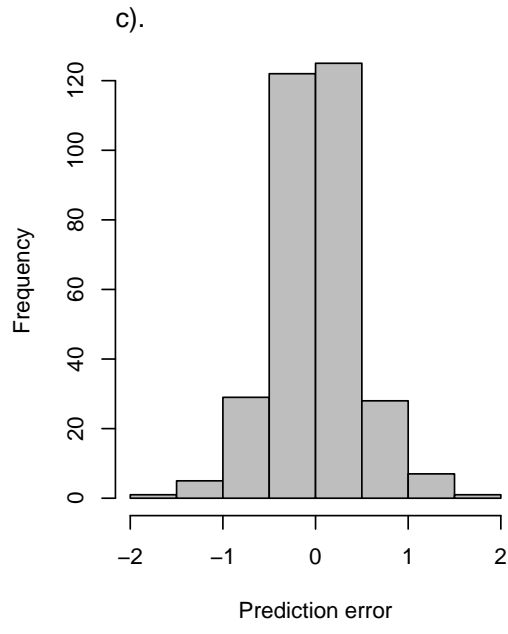
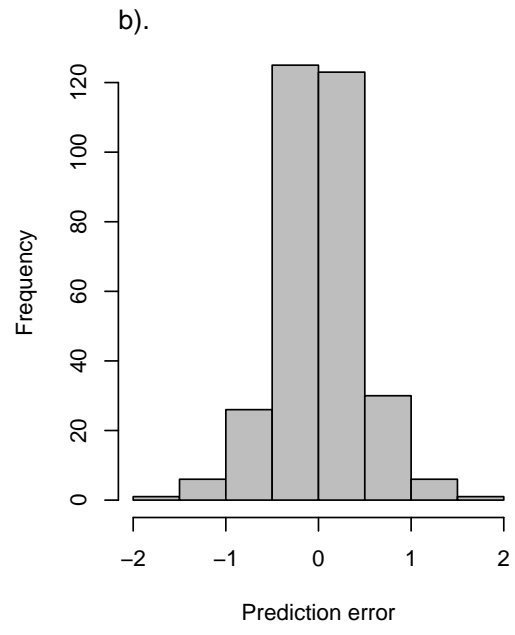
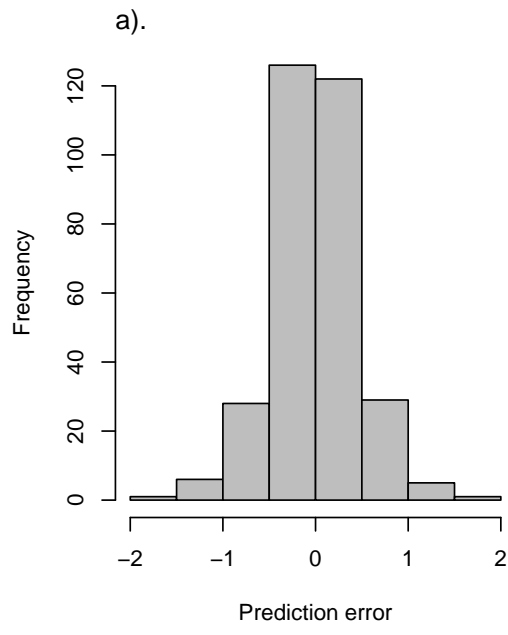
2: Fig 1



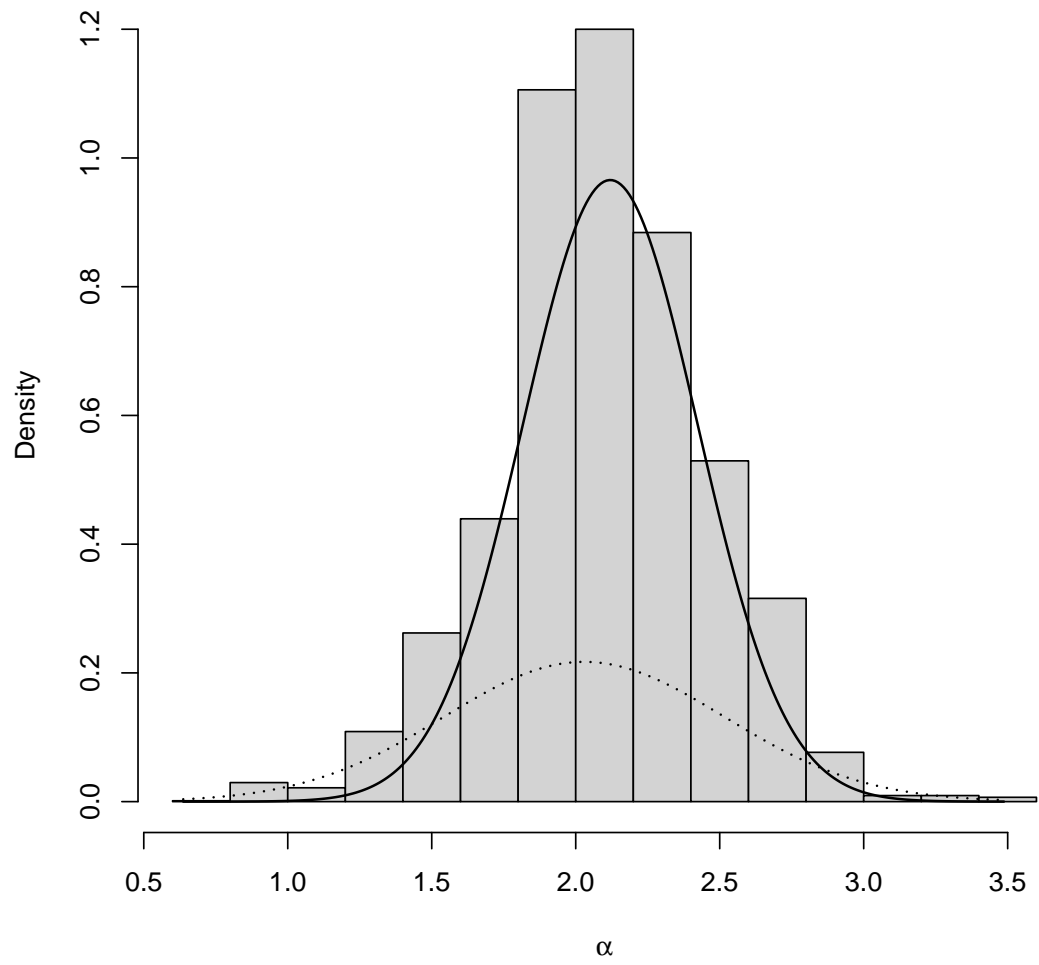
3: Fig 3



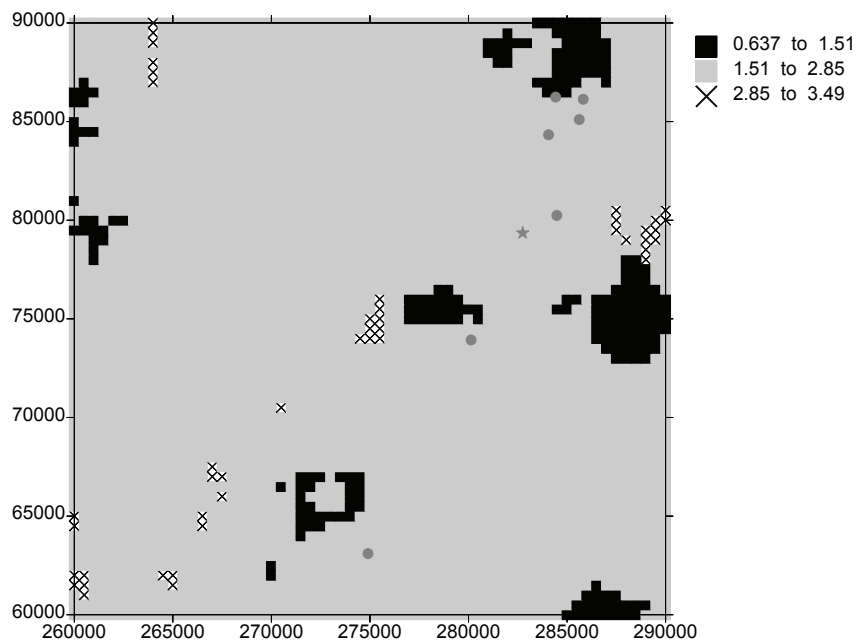
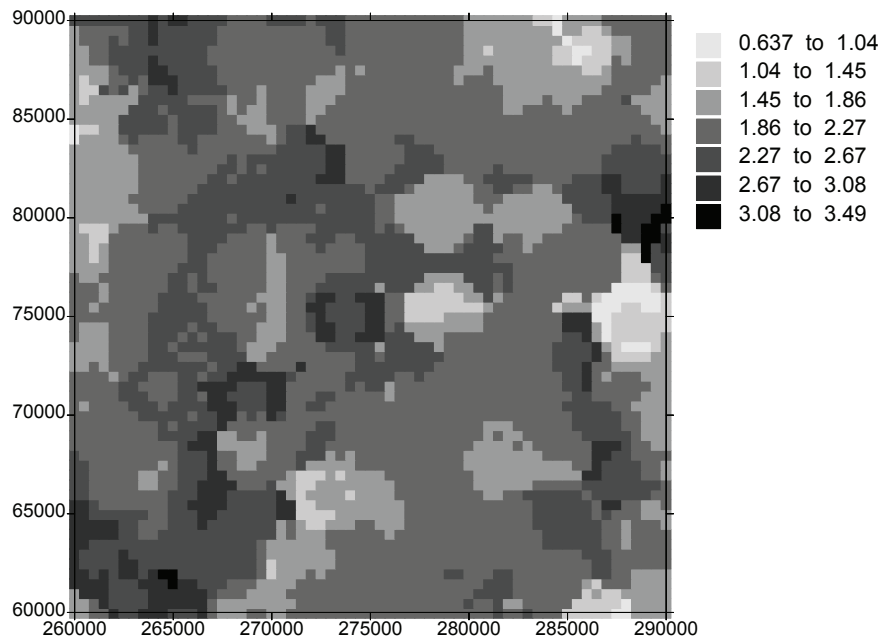
4: Fig 4



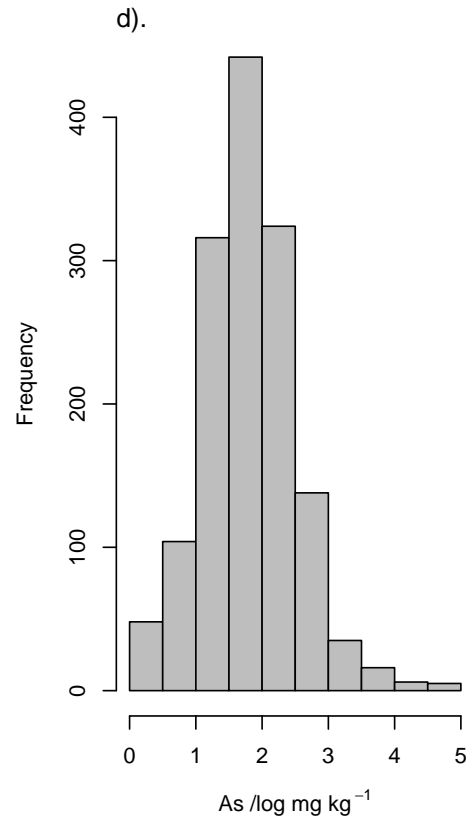
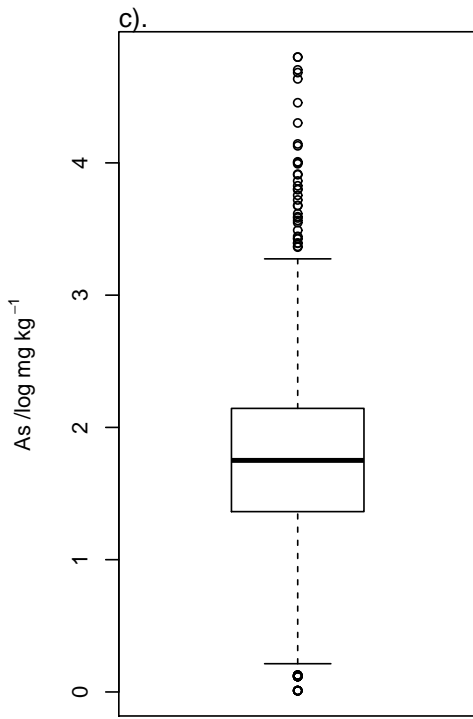
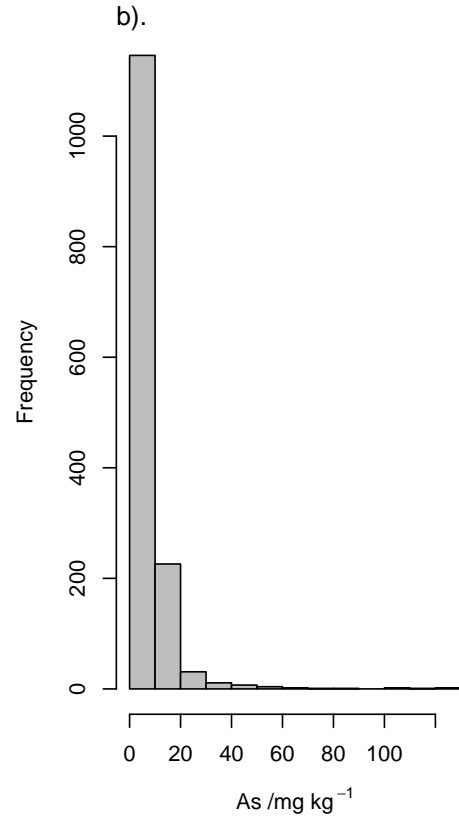
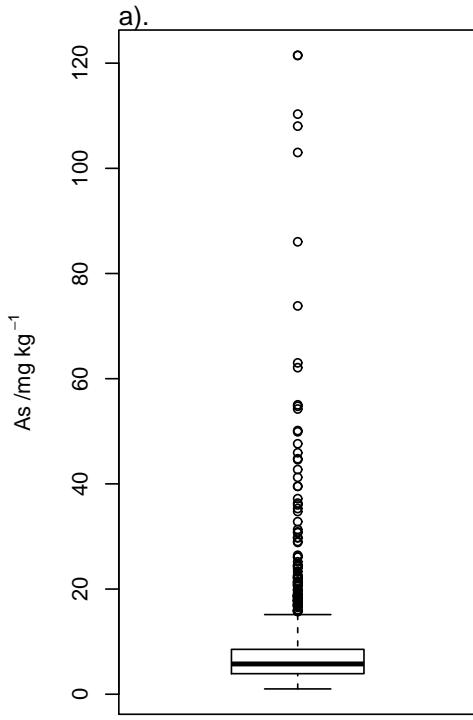
5: Fig 5



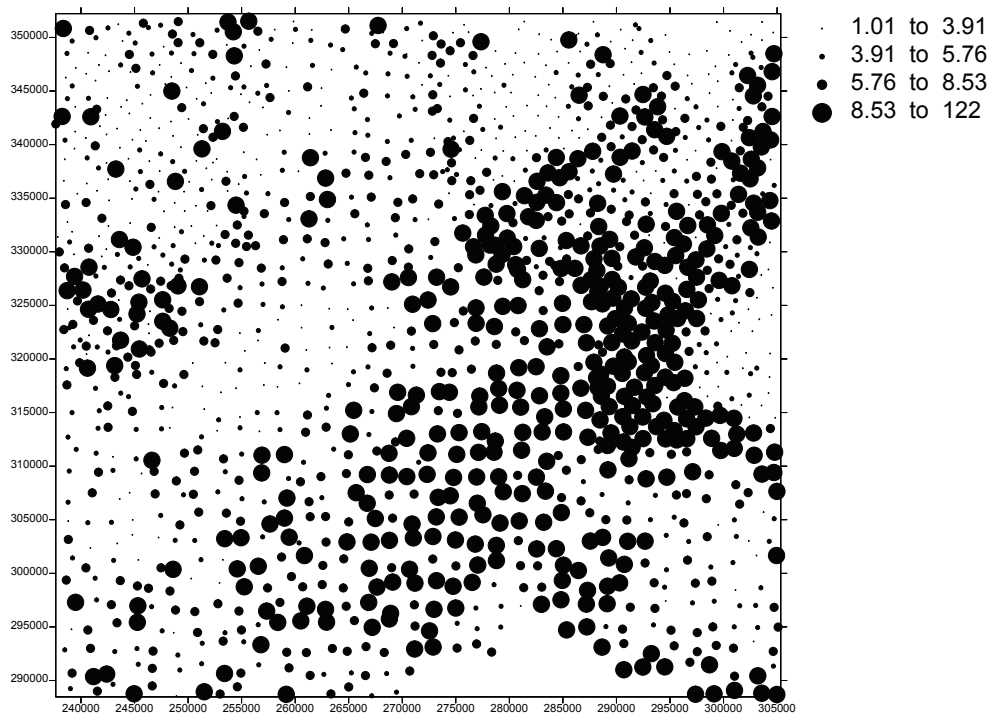
6: Fig 6



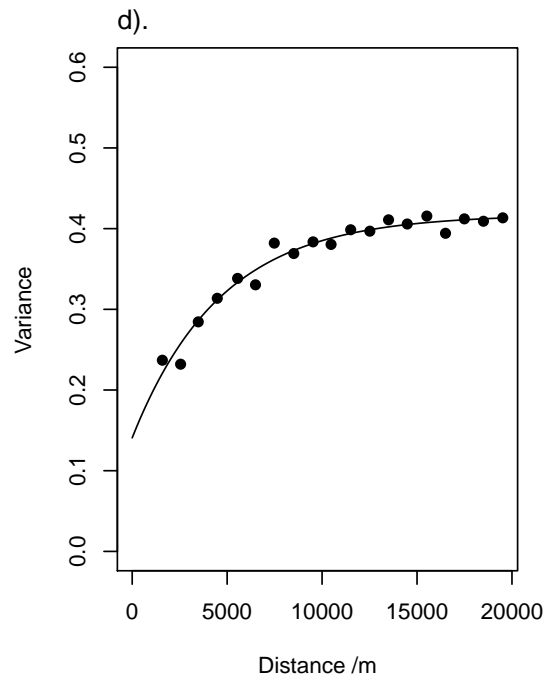
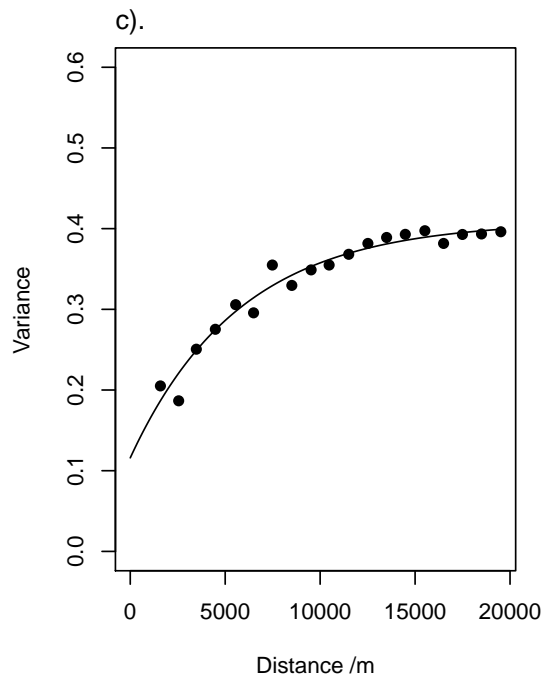
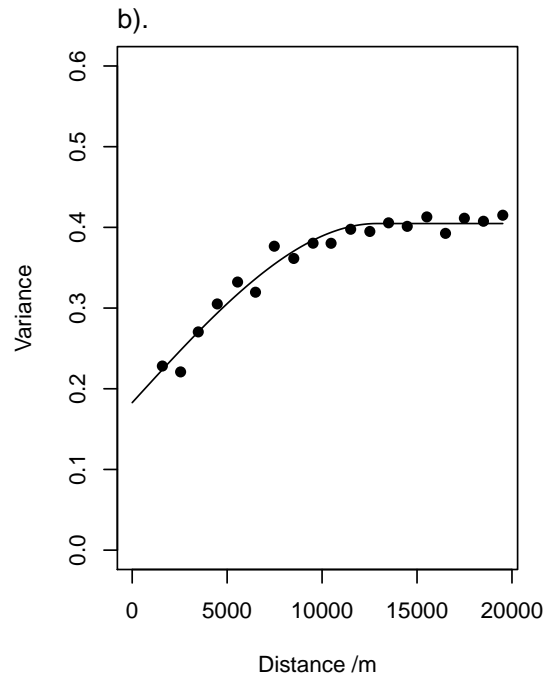
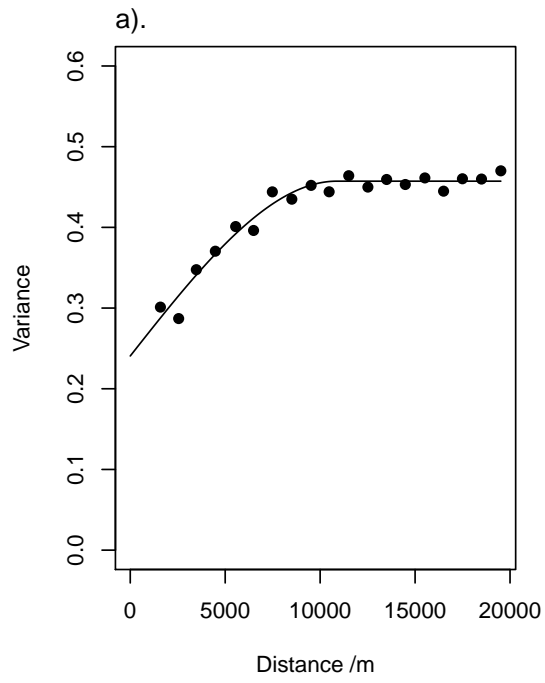
7: Fig 7



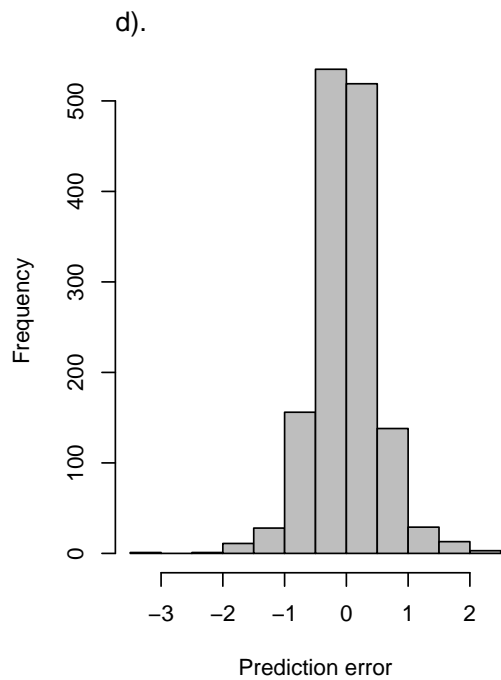
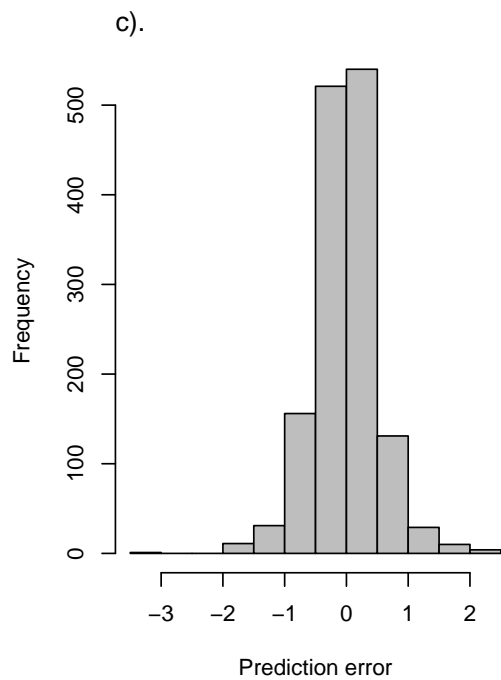
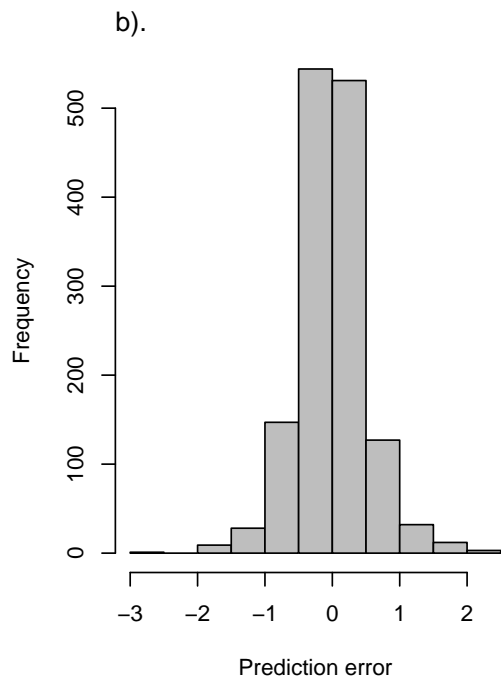
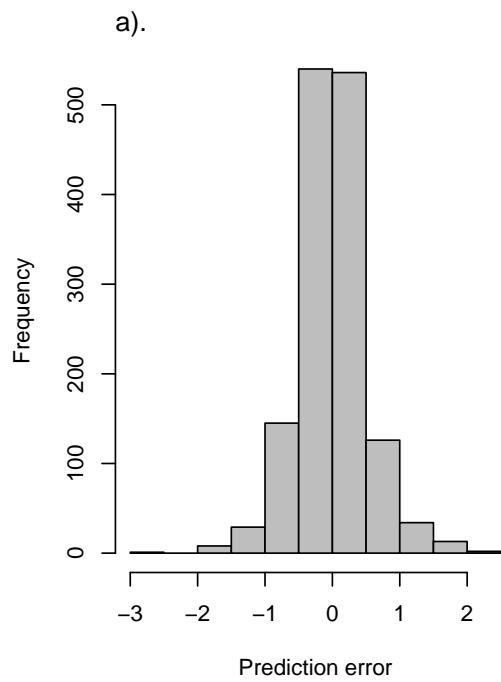
8: Fig 8



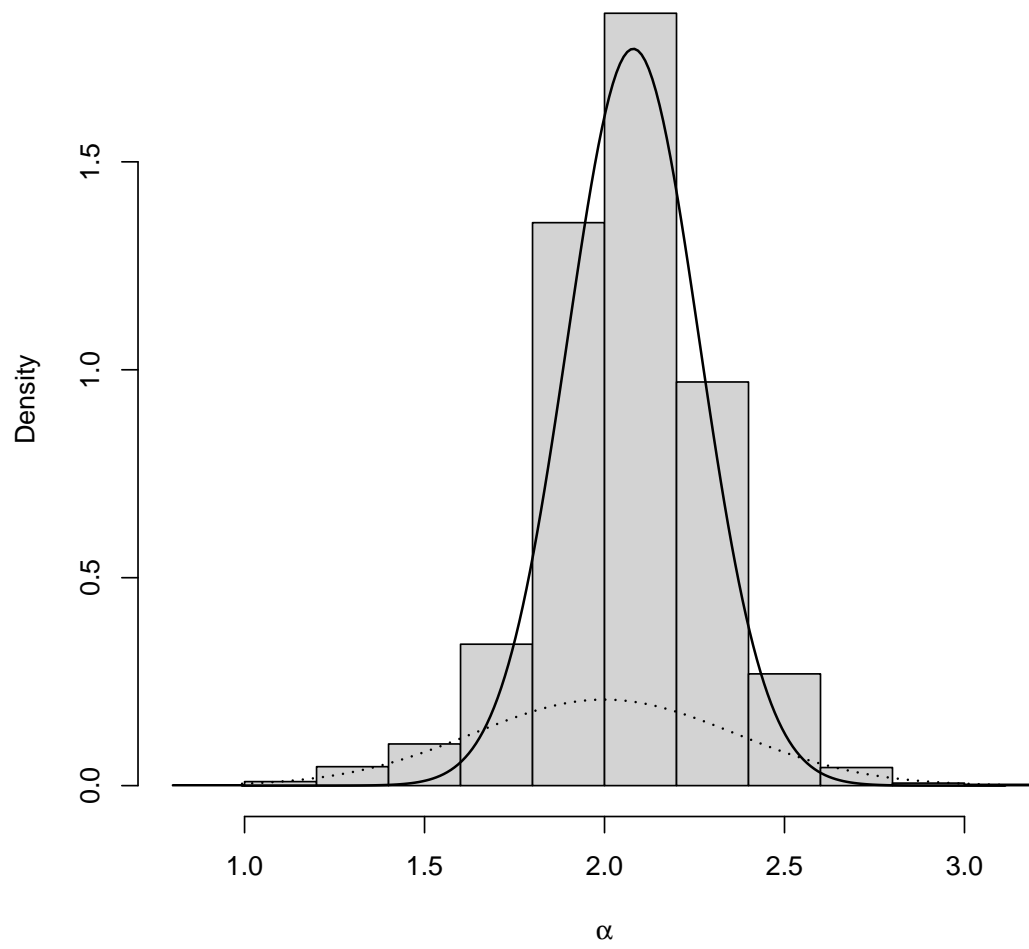
9: Fig 9



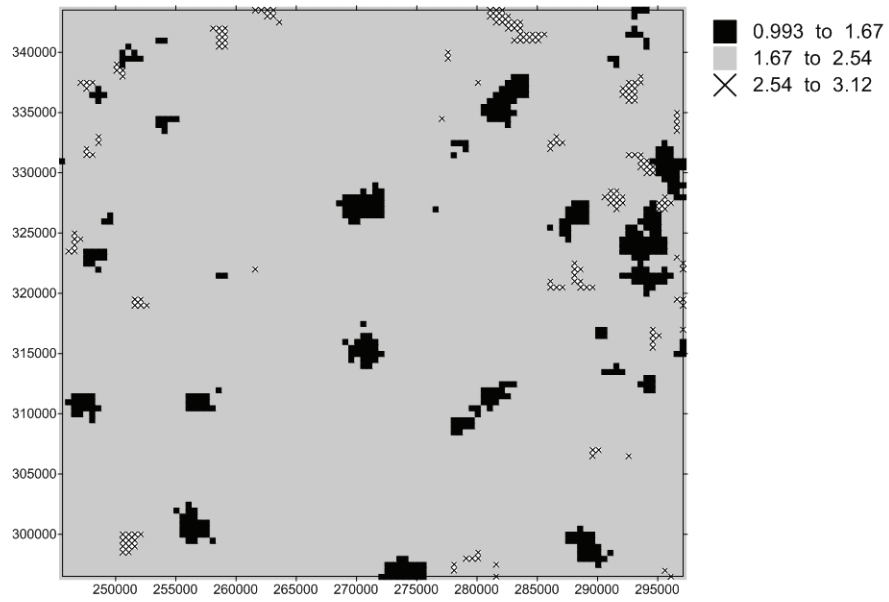
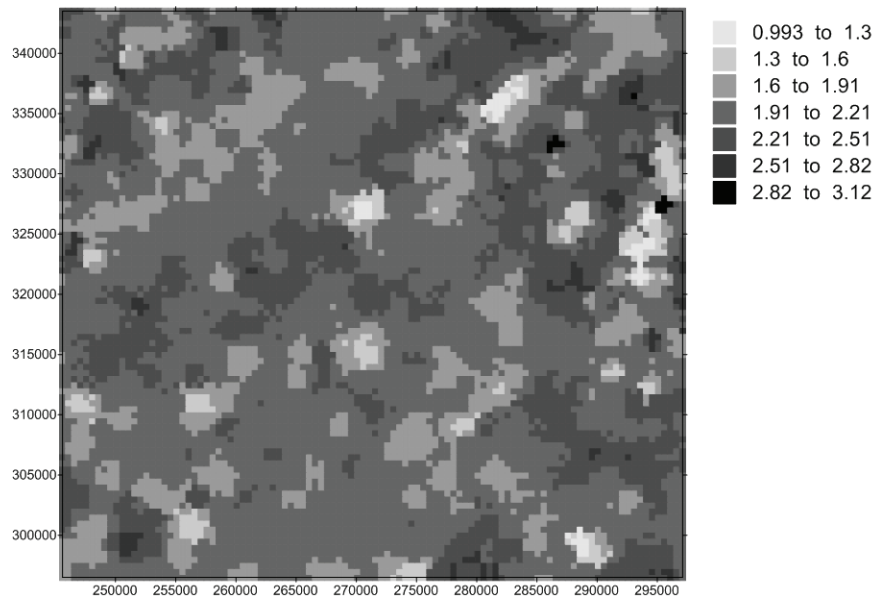
10: Fig 10



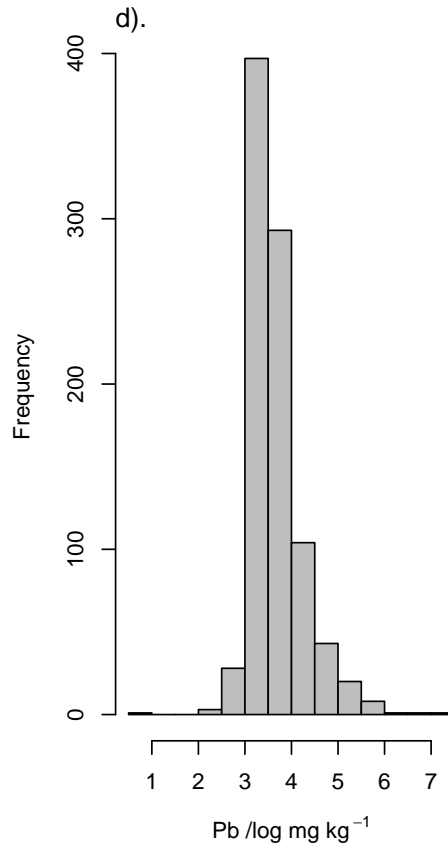
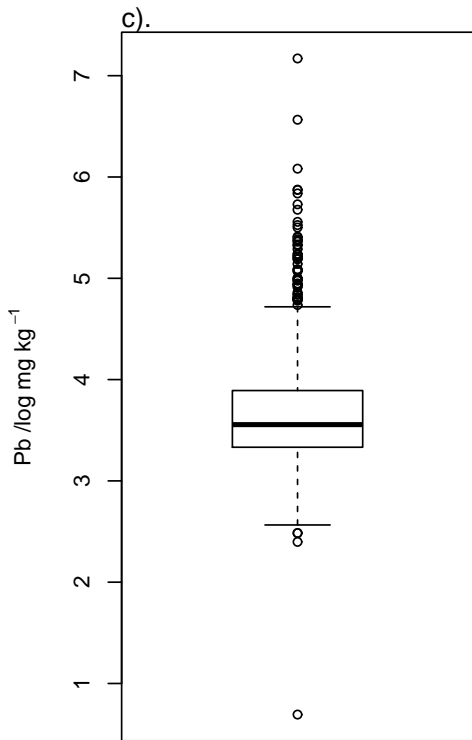
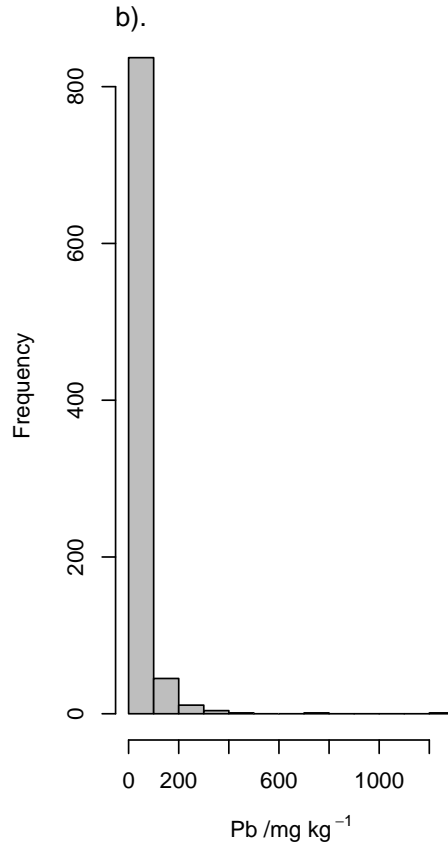
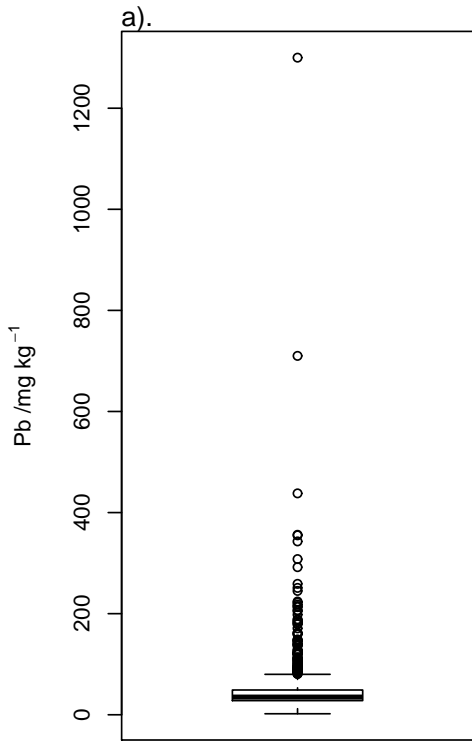
11: Fig11

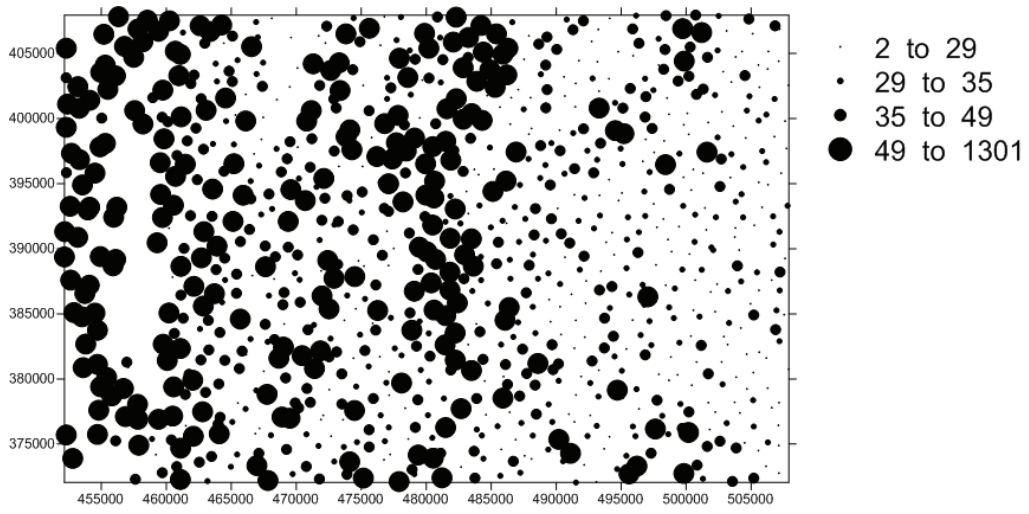


12: Fig 12

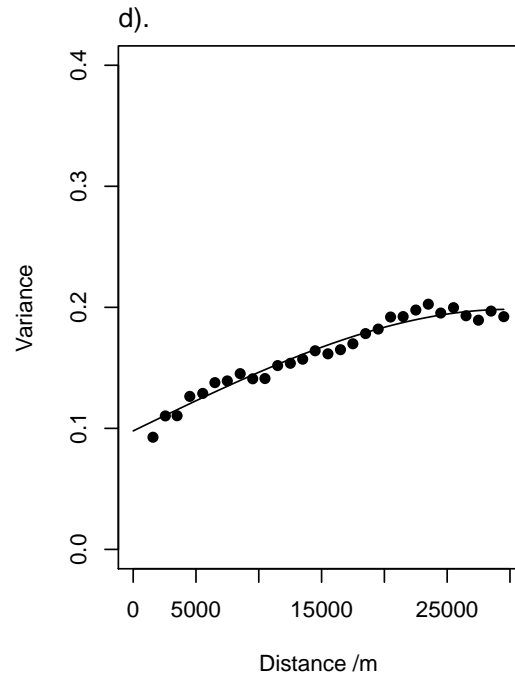
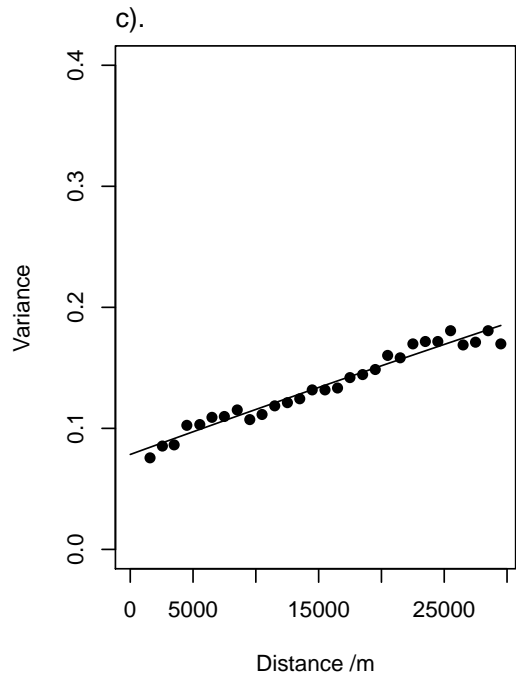
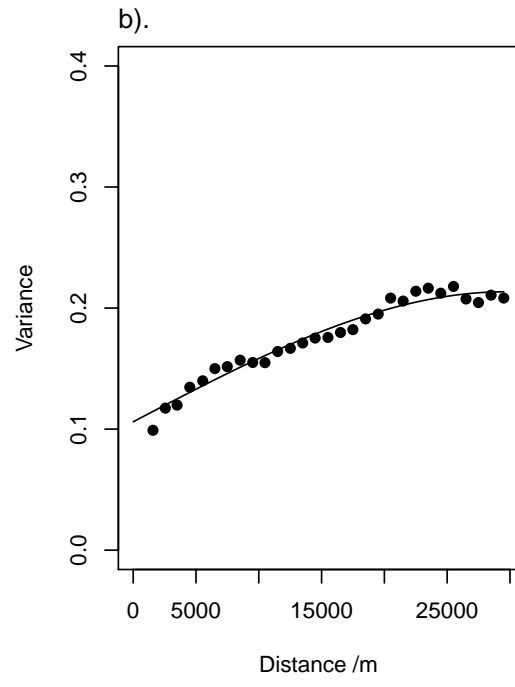
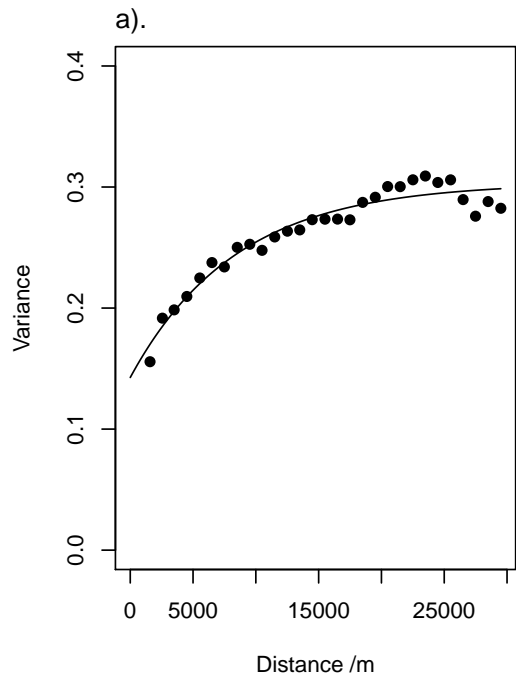


13: Fig 13

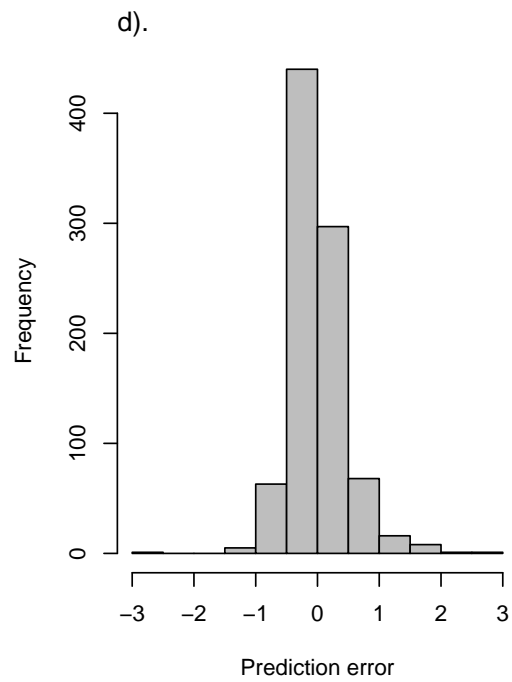
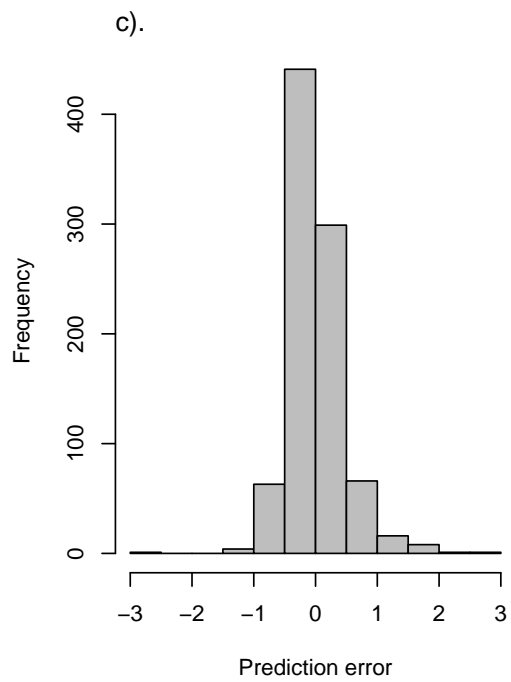
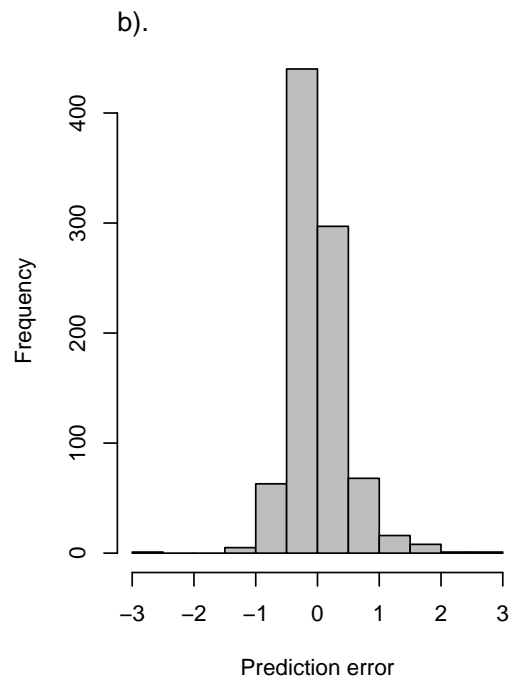
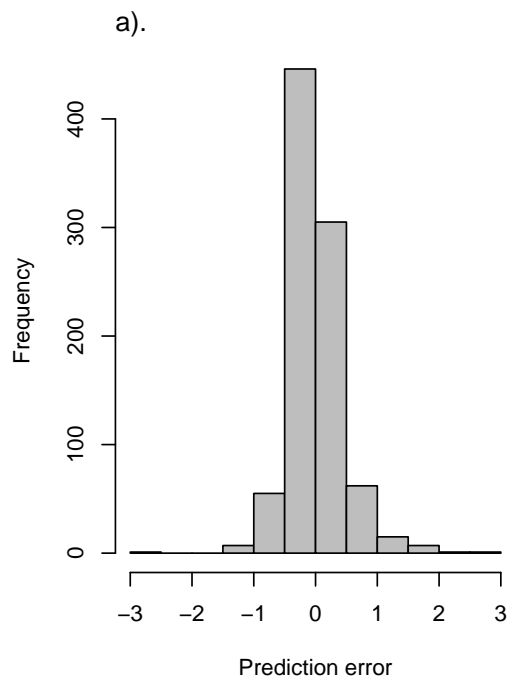




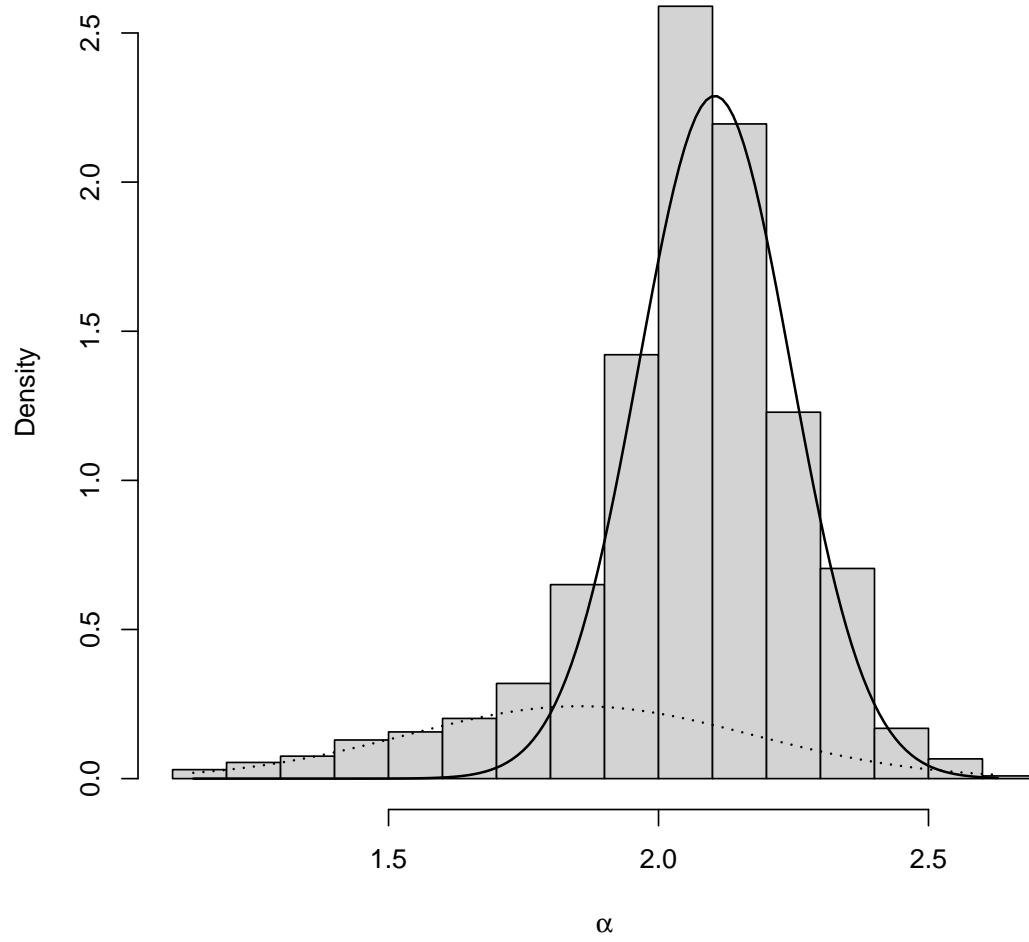
15: Fig 15



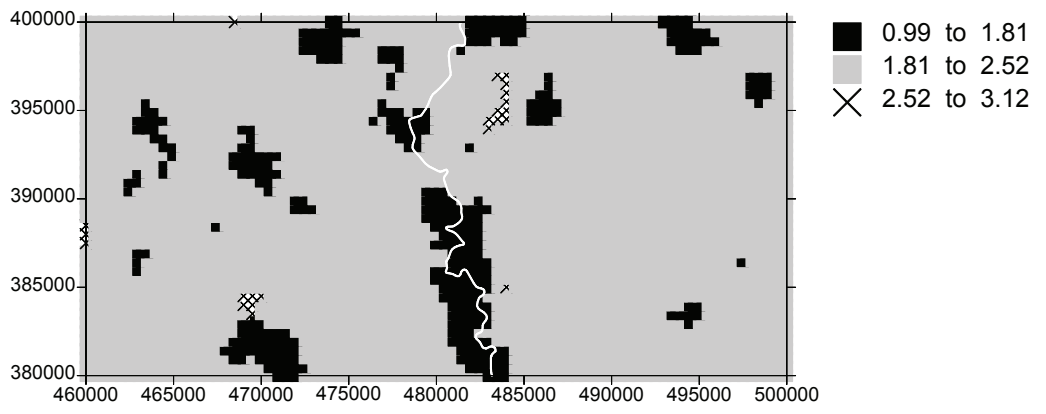
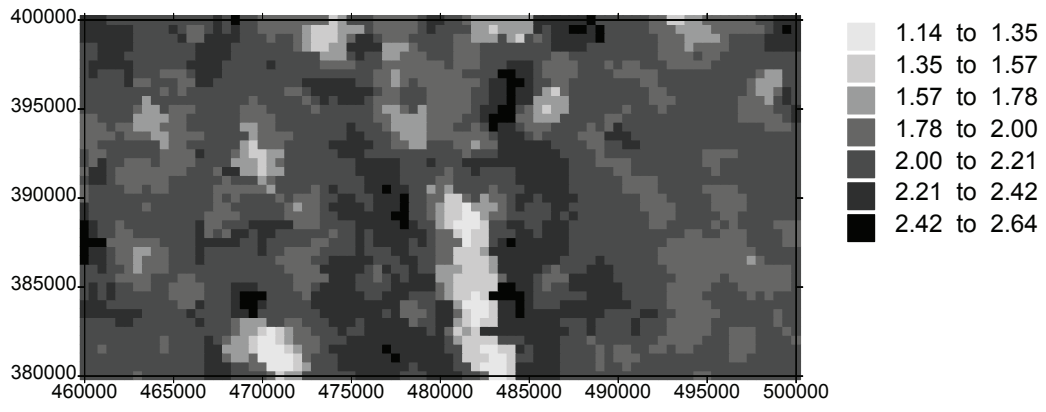
16: Fig 16



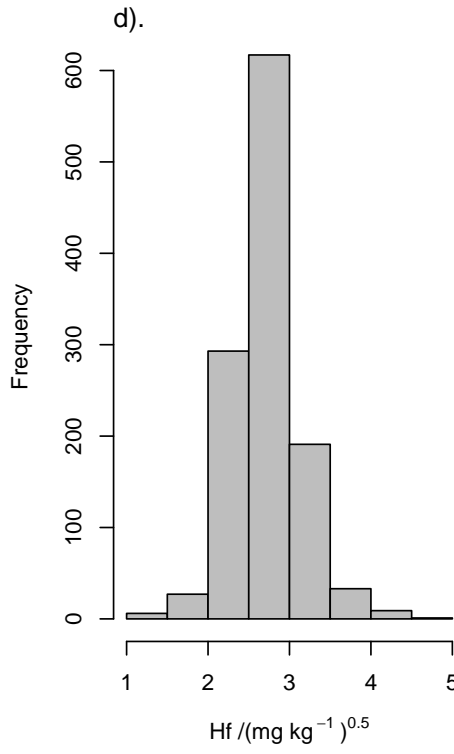
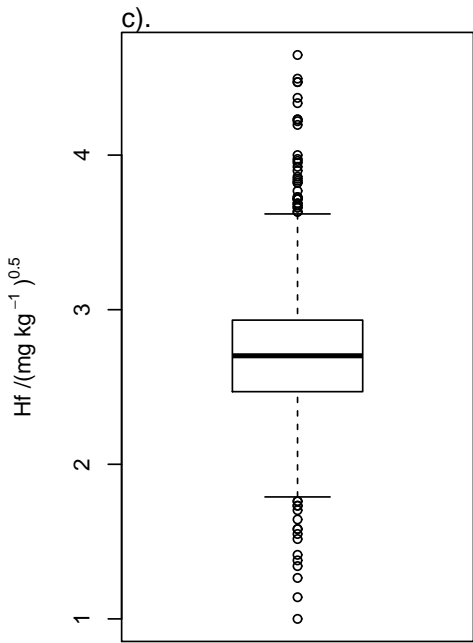
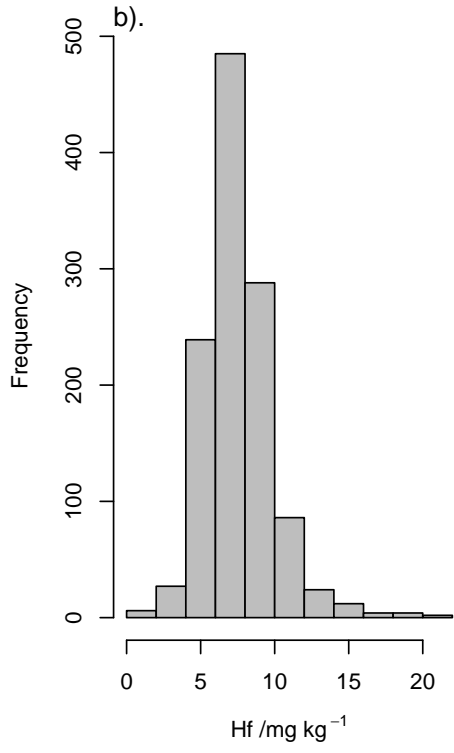
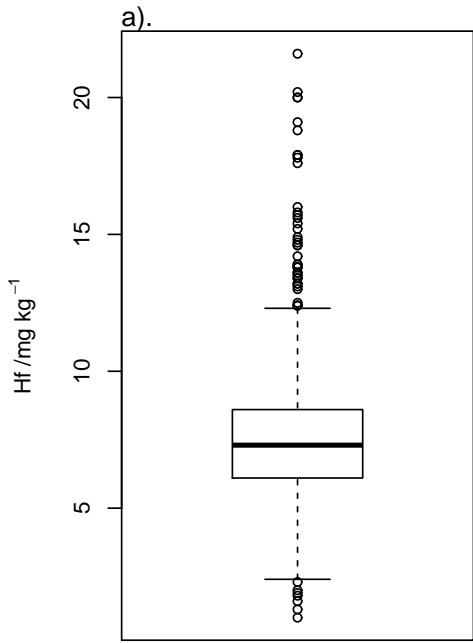
17: Fig 17



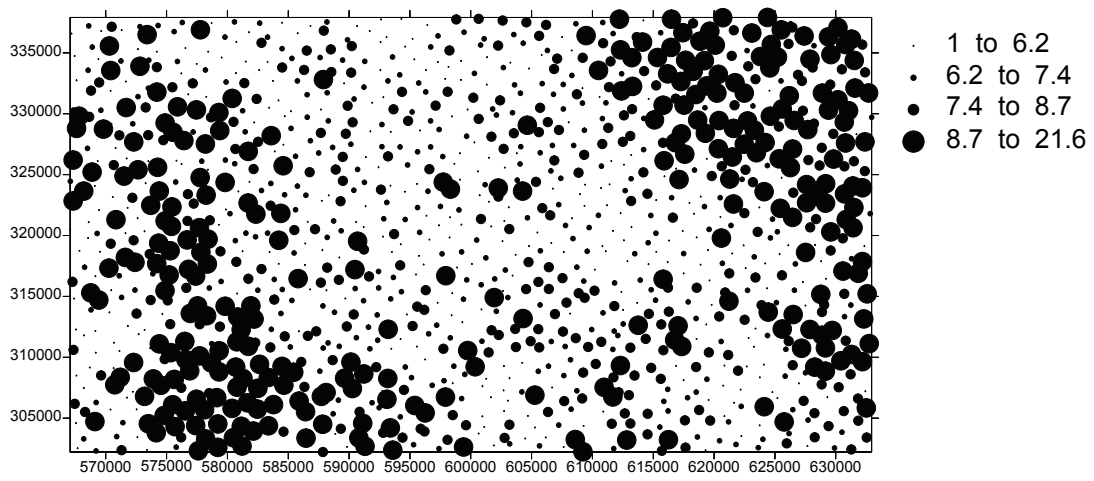
18: Fig 18



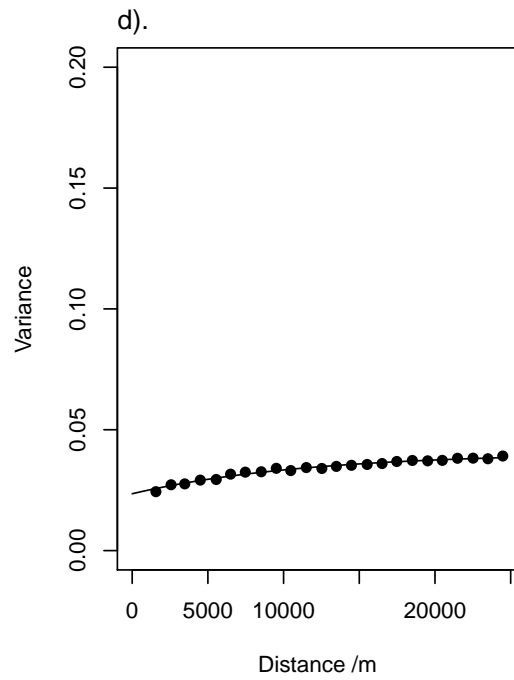
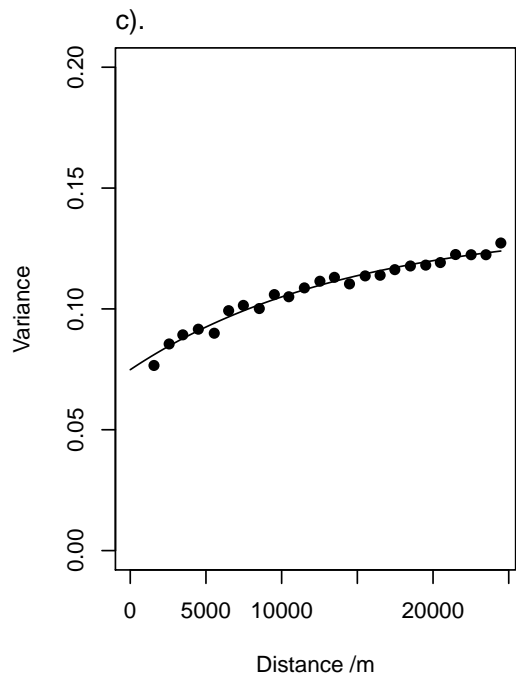
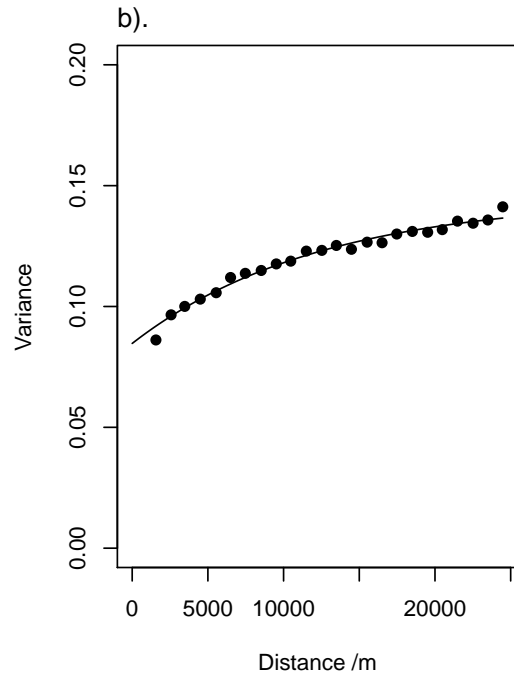
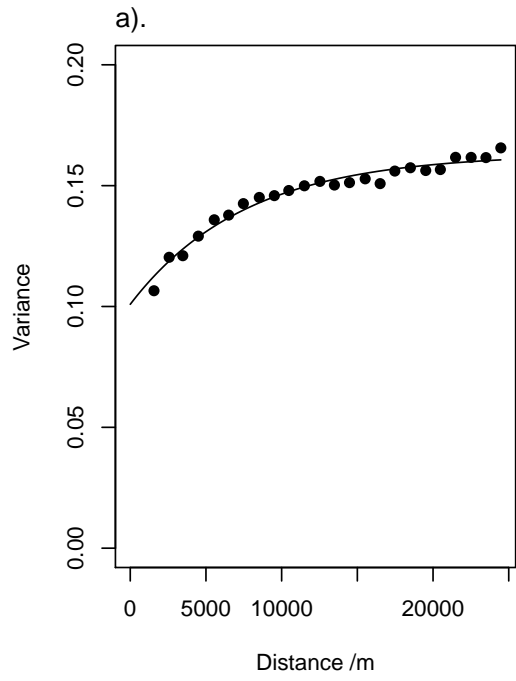
19: Fig 19



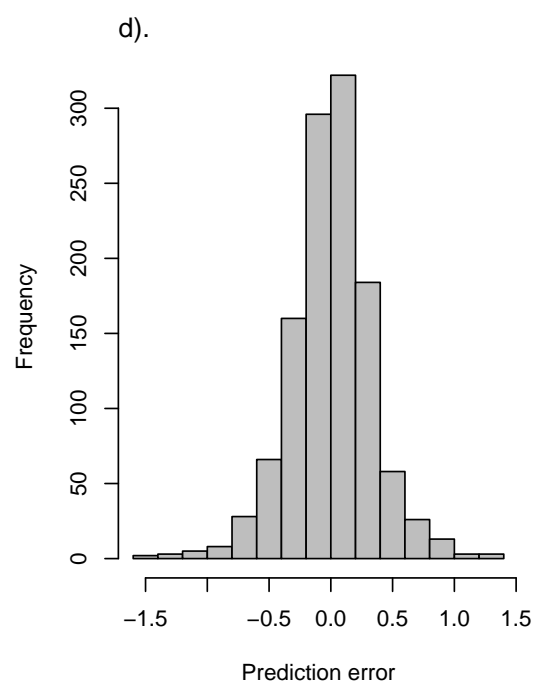
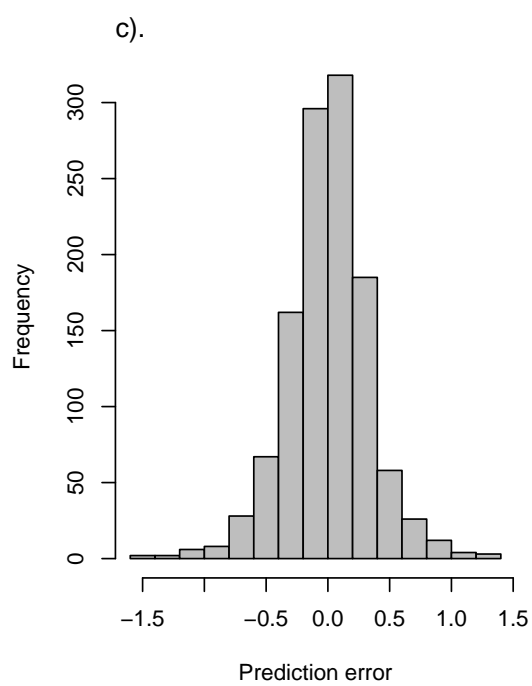
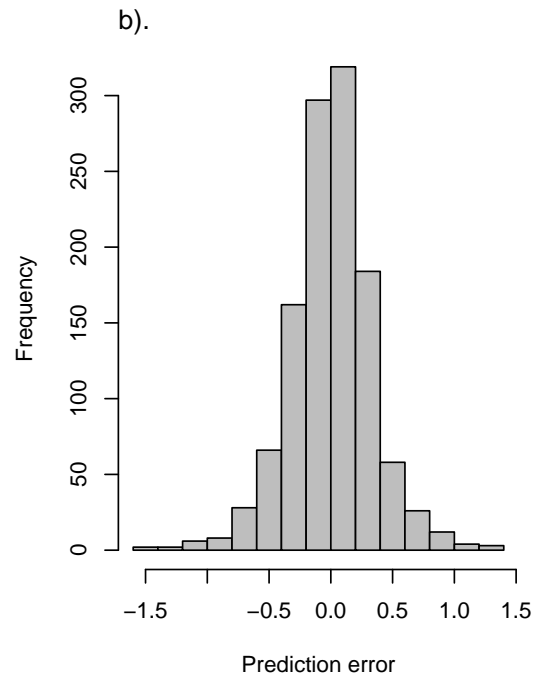
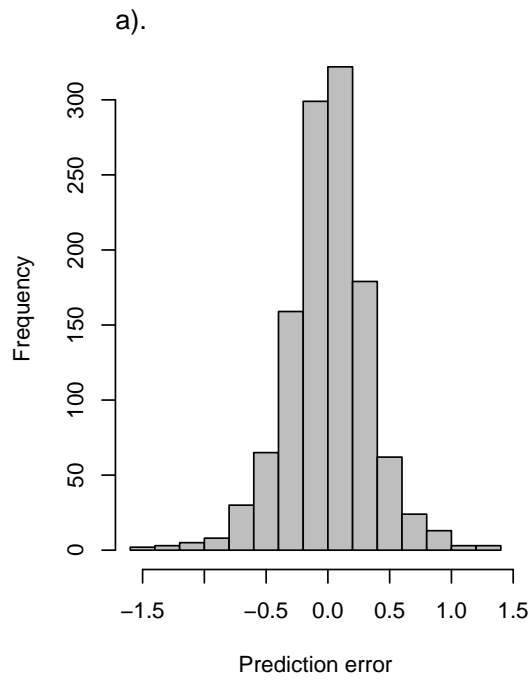
20: Fig 20



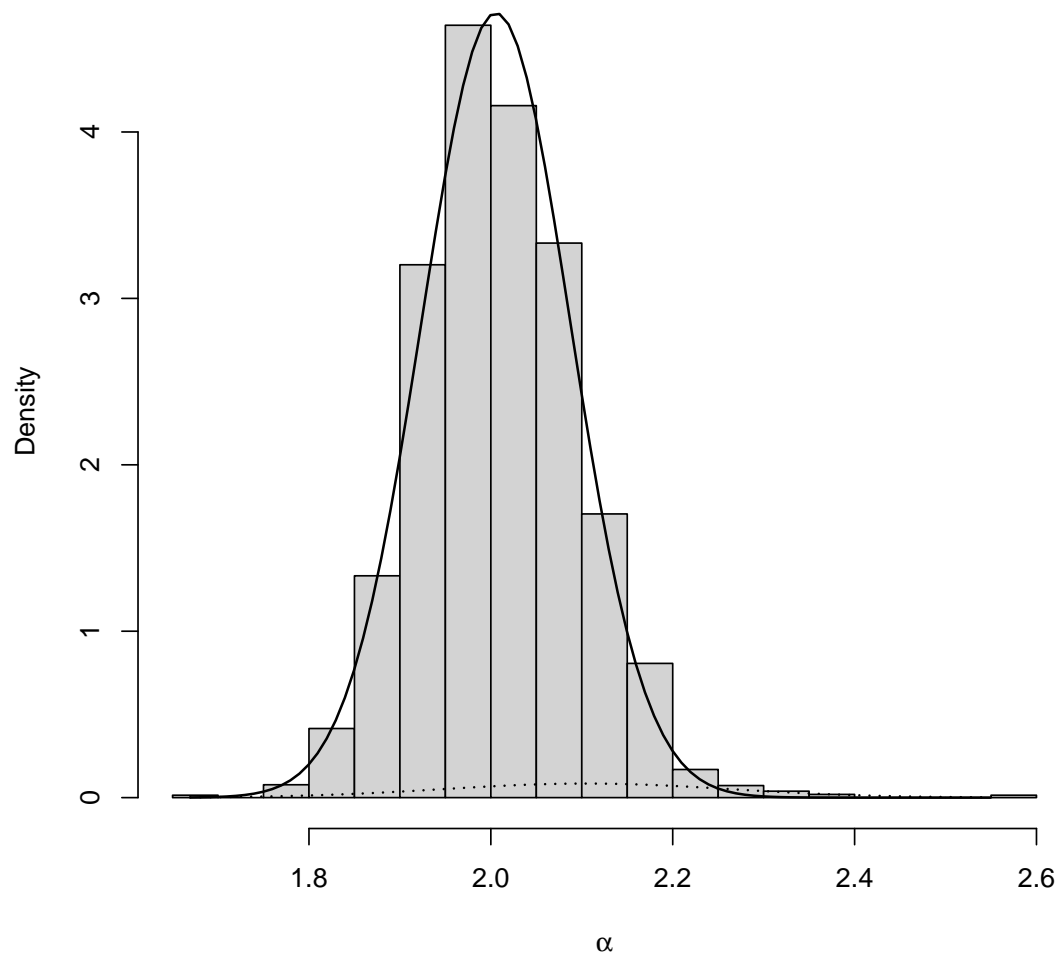
21: Fig 21



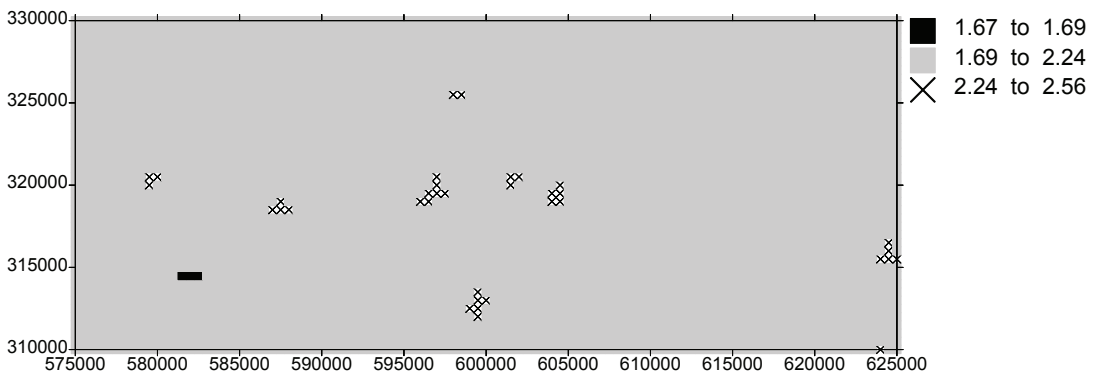
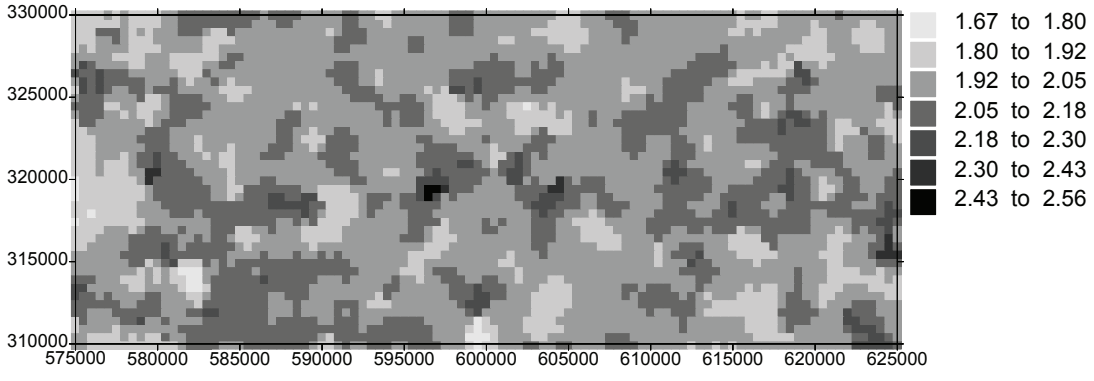
22: Fig 22



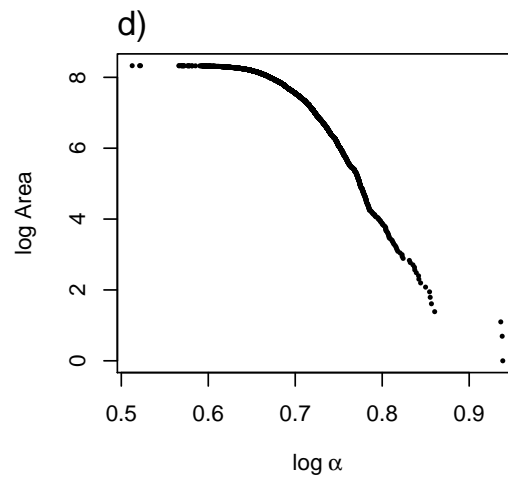
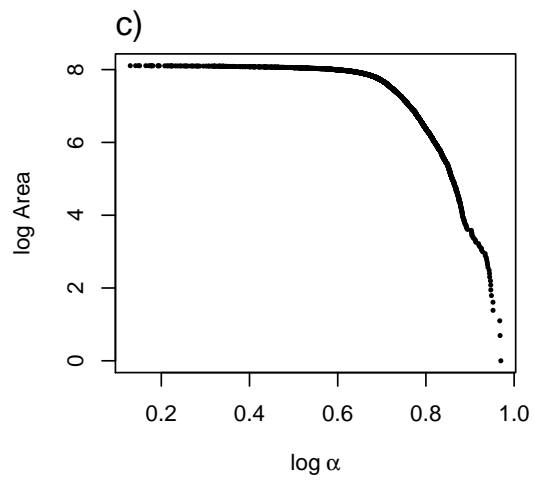
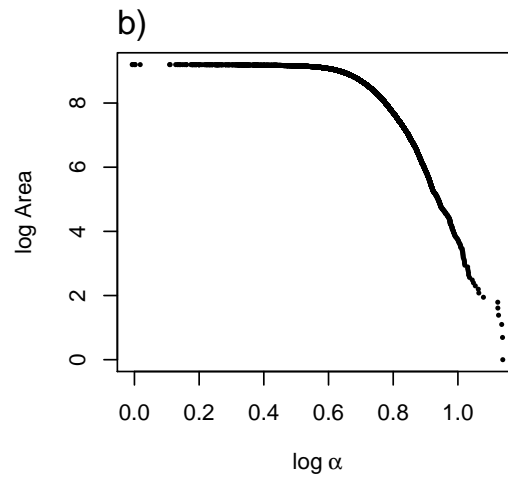
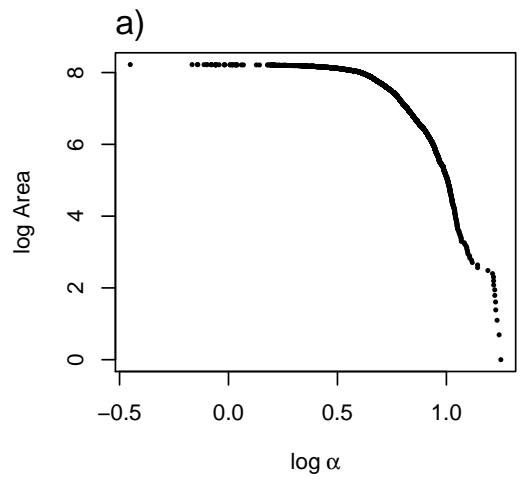
23: Fig 23



24: Fig 24



25: Fig 25



26: Fig 26